Fermilab

Optimization for $\nu_\mu \rightarrow \nu_\tau$ appearance in DUNE

Letizia Parato

Università degli Studi di Torino

Italian Students Internship

25 july - 23 september 2016

Supervisor

Alberto Marchionni

DEEP UNDERGROUND NEUTRINO EXPERIMENT

Contents

Framework **2**

1 Introduction **3**

2 DUNE/LBNF **4**
2.1 Scientific goals . . . 4
2.1.1 The Primary Program . . . 4
2.1.2 The Ancillary Program . . . 4
2.1.3 The Additional program . . . 5
2.2 Near site facilities . . . 5
2.2.1 Reference and Optimized design . . . 6
2.2.2 The magnetic horns . . . 7
2.2.3 The near detector . . . 8
2.3 Far site facilities . . . 8
2.3.1 The far detector . . . 8

3 Neutrino oscillations **9**
3.1 Massive neutrinos and PMNS mixing matrix . . . 9

4 Neutrino detection **12**

My work **14**

5 G4LBNE software **15**
5.1 Issues with oscillated ν_τ CC events rate histograms . . . 16

6 Results of simulations **17**
6.1 Optimized and default reference designs . . . 17
6.2 Placing the target and the second horn . . . 18
6.2.1 2013 vs. 2016 neutrino oscillation parameters . . . 20
6.3 Rescaling the second horn . . . 20
6.4 Modifying the target . . . 22
6.4.1 Multi spheres target . . . 23
6.4.2 Cylindrical target . . . 23

7 Neutrino flux analysis **25**

8 Conclusions **28**

Chapter 1

Introduction

The ν_τ was postulated to exist after the discovery of the τ lepton in 1975 and its discovery was announced in 2000 by the DONUT collaboration. For now, only 9 ν_τ CC events from via decay of charmed mesons (DONUT) and 5 ν_τ CC events from oscillation of ν_μ neutrinos (OPERA) have been detected. With its huge fiducial mass, high resolution and opportunity to make accurate calorimetric measurements, the DUNE LArTPC (section 2.3.1) far detector offers the possibility to identify the tau appearance with high fidelity and to greatly improve the collection of ν_τ events. It is reasonable to think of a ν_τ appearance experiment taking place after the conclusion of the low-energy experiments related to the primary scientific program (section 2.1.1).

To obtain the best results from the ν_τ appearance experiment it is necessary to make changes to the default reference design (section 2.2.1). This involves modifying the placement of the target and the position of the horns, rescaling the second horn and changing the length, the width and the type of target. The goal is to find the set of parameters which maximizes the number of oscillated ν_τ charge-current events at DUNE far detector.

My contribution After checking the cross-sections data and the oscillation probability calculator code, I modified eventsRate, the piece of code that makes ν_τ oscillated flux histograms, in order to make it read ν_τ and $\bar{\nu}_\tau$ cross-sections and built the correct ν_τ CC events rate histogram (section 5.1). Then I updated the oscillation parameters to 2016, I build the macros and I ran the simulations (chapter 6). In the end, I analysed the double peak (chapter 7) visible in the ν_μ flux to understand where it came from.

Chapter 2

DUNE/LBNF

DUNE is a long term physics program which aims to the measurement of unknown parameters of the Standard Model of particle physics and the search for new phenomena. The Long-Baseline Neutrino Facility (LBNF), the facility required for the experiment, will be hosted at Fermilab. The experiment will comprise the world high-intensity neutrino beam, a high precision near detector at Fermilab, in Batavia, IL and a liquid Argon time projection chamber (LArTPC) far detector at the Sanford Undergroung Research Facility (SURF) in Lead, SD. The far detector will be 1300 km far from the neutrino beam origin.

2.1 Scientific goals

The main focus of the scientific program is the demonstration of leptonic CP violation by measuring differences between oscillations of muon-type neutrinos into electron-type neutrinos and of muon-type antineutrinos into electronic-type antinuetrinos and the determination of the neutrino mass hierarchy. Additional research opportunities could be unlocked by the high precision of the deep underground far detector. The DUNE/LBNF scientific goals can be separated in three categories:

- **Primary program** the primary mission of the experiment.
- **Ancillary program** for which will be necessary to modify LBNF design from the design that will be adopted for the primary program, in particular changes to the near detector, to the shape and placement of the horns and to the design and placement of the target will be needed.
- **Additional program** that requires developments of the LArTPC technology.

2.1.1 The Primary Program

1. Precision measurements of the parameters that govern $\nu_\mu \to \nu_e$ and $\bar{\nu}_\mu \to \bar{\nu}_e$ oscillations with the aims enumerated below.
   (a) Measuring the CP violating phase. A value different from 0 or π would represent the discovery or the confirmation over 5σ of the CP–violation in the leptonic sector, providing a possible way to explain the matter-antimatter asymmetry in our universe.
   (b) Determining the sign of $\Delta m^2_{13} = m^2_3 - m^2_1$, i.e. the mass hierarchy.
   (c) Precision tests of the three-flavour neutrino oscillation paradigm studying ν_μ disappearance and ν_e appearance with the measurements of neutrino fluxes, including the measurement of θ_{23} angle and the octant in which this angle lies.
2. Search for proton decay in many possible decay modes. The proton decay, if observed, would be a revolutionary discovery and would provide a chance to the grand unification of the forces.
3. Detection of ν_e flux from core-collapse supernova, if such an event occur in our galaxy during the experiment's lifetime.

2.1.2 The Ancillary Program

1. Other neutrino flavour transition measurements such as
   (a) non-standard interactions,

(b) the search for sterile neutrinos,

(c) the measurement of tau neutrino appearance.

2. Neutrino interactions measurements using DUNE near detector, such as

   (a) measurements of neutrino cross-sections,

   (b) studies of nuclear effects on the neutrinos detection,

   (c) measurements of the structure of nucleons,

   (d) measurements of the weak angle.

3. Physics of atmospheric neutrinos.

4. Search for signatures of dark matter.

2.1.3 The Additional program

1. Measurements of neutrino oscillation phenomena and of solar physics using solar neutrinos.

2. Measurement of neutrinos from astrophysical sources at energies from active galactic nuclei, gamma-ray bursts, black-hole and neutron-star mergers.

3. Detection and measurement of the diffuse supernova neutrino flux.

2.2 Near site facilities

The design is a conventional, horn-focused neutrino beamline. A proton beam is extracted at Fermilab Main Injector (MI) and transported into the target hall that hosts the target and the magnetic horns. Here the proton beam is directed to a target area where the collisions generate charged particles (mainly pions, then kaons and muons) that are focused by the horns.

The charged particles are diverted to the decay tunnel, a pipe of circular cross section with its diameter and length optimized such that decays of the pions and kaons result in neutrinos in the energy range useful for the experiment. The charged particles decay (e.g., $\pi^+ \to \mu^+ + \nu_\mu$) producing the neutrino beam directed towards the detectors.

The decay tunnel is followed immediately by the absorber, which removes the remaining beam hadrons.

The near detector facilites include a small muon alcove area in the beamline absorber hall and a separate underground near detector hall that houses the near detector.

The facility is designed for initial operation at a proton-beam power of 1.2 MW, designed to support an upgrade to 2.4 MW. Operation of the facility is planned for twenty years, while the lifetime is planned for thirty years.

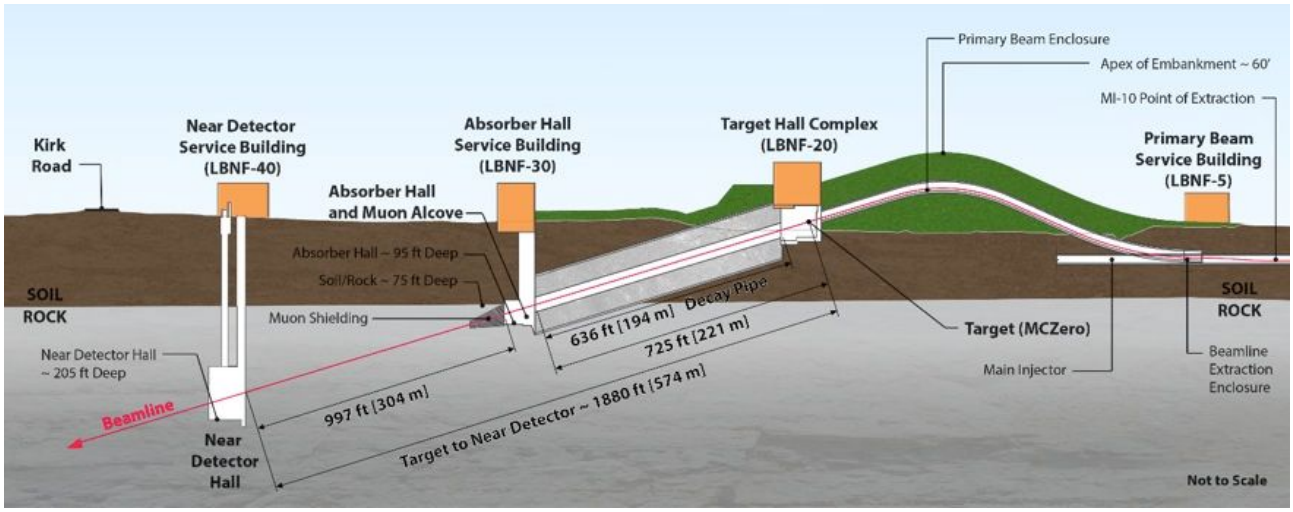

2.2.1 Reference and Optimized design

There exist two different designs on the LBNF neutrino beamline: the reference design and the optimized design. The reference design is based on the designs of targets and focusing systems for NuMI. It consists of two parabolic horns, the second larger then the first, and a graphite target. The target consists of 47 segments, for a total length of 95 cm including a space of two interaction lengths between segments. The upstream face of the first segment is positioned 45 cm upstream of the first focusing horn and the separation of the upstream faces of the two horns is 6.6 m. A helium-filled decay pipe, 4 m in diameter and 204 m in length, provides the decay volume for the neutrinos parent particles to decay to ν_μ.

The reference design is well understood, have proven high performance and reliability and it is the one proposed in the first LBNF/DUNE Conceptual Design Report. In the same paper it is also demonstrated that the optimization of the beam design (i.e. optimization of the target and the focusing system) can be essential to achieve the goals listed in the primary program, independent of additional improvements to the accelerator complex such as power and efficiency improvements.

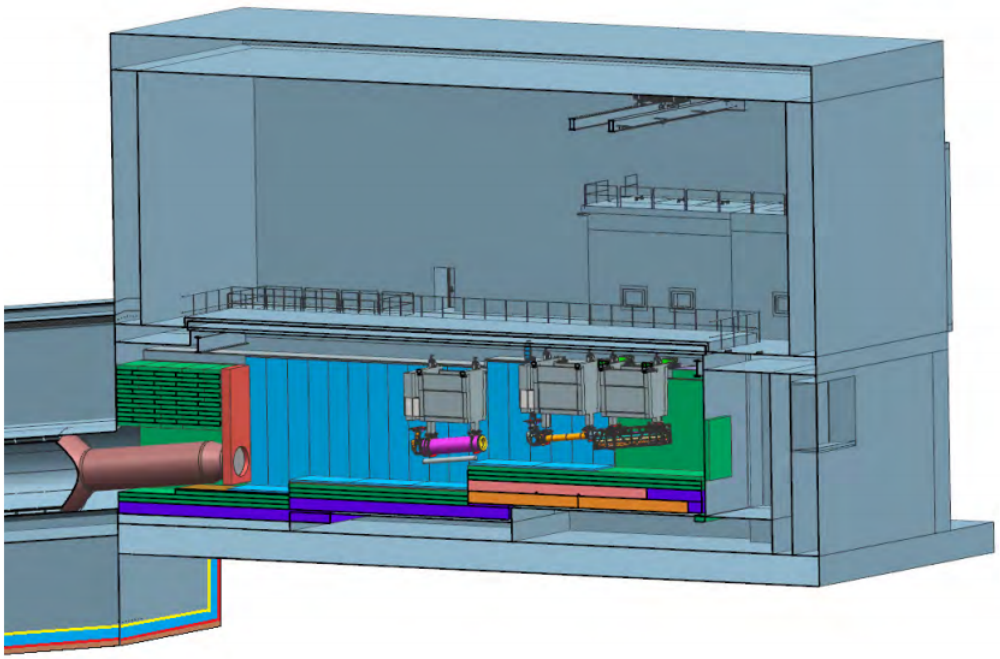

Figure 2.1: Target hall in the reference design (right to left: target, horn 1 in orange, horn 2 in pink, decay pipe window in red followed by the beginning of the decay pipe)

The optimized design, still undergoing improvements, consists in three conical horns. The horn inner conductors are combinations of cylindrical and conical sections and the graphite target, larger then the NuMI target, is located into the first horn's inner conductor.

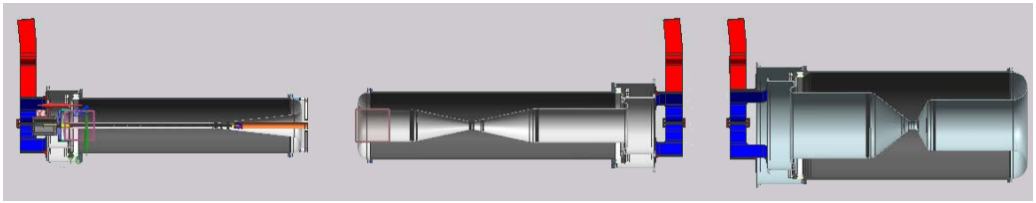

Figure 2.2: Optimized design (left to right: horn A with target inside, horn B and horn C)

The optimized design, despite its efficiency for the measurements enumerated in the primary program, is not suitable for ν_τ appearance observation. In fact the ν_μ flux is higher but less energetic in the optimized design than in the reference design. Therefore, since high energy neutrinos are needed to make τ leptons appear at far detector, it would be better to use a design similar to the reference design for the ν_τ appearance experiment.

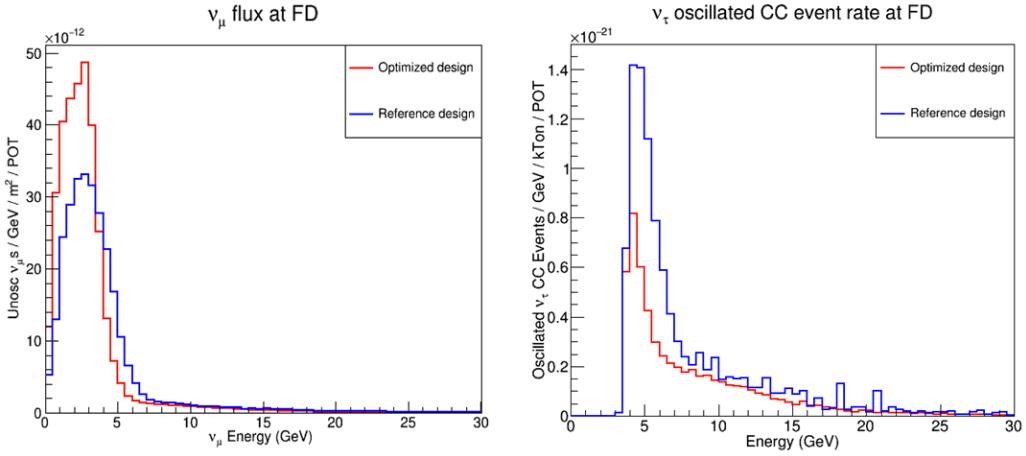

2.2.2 The magnetic horns

The idea of the magnetic horn was developed by Simon van der Meer in 1961. A magnetic horn is a focusing device build to collect pions and kaons generated into the target and direct them toward the detectors, increasing in this way the neutrino flux. The horn consists of two coaxial and axial-symmetric conductors; the current runs in the axis direction in two opposite sides in the inner and in the outer conductor in order to generate an azimuthal toroidal magnetic field. Here the Lorentz force $q\vec{v}\times\vec{B}$ acts on the charged particles defocusing minus-charged (plus-charged) particles and focusing plus-charged (minus-charged) particles if the horn is working in neutrino (antineutrino) mode thus enhancing a ν_μ ($\bar{\nu}_\mu$) beam an reducing the $\bar{\nu}_\mu$ (ν_μ) background.

Conical horns

It refers to a horn whose inner conductor has a conical surface. Such device focuses all momenta for a fixed angle $\theta_{in} = r/l$ of pion into the horn.

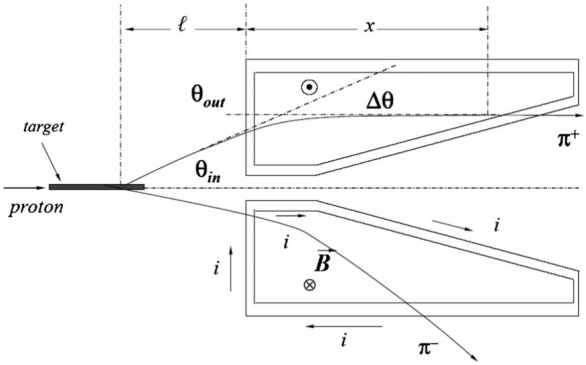

Parabolic horns

It refers to a horn whose inner conductor has a parabolic-shaped surface. Such a device focuses a given momentum for all possible angles of entry of the particle into the horn. To see this, note first that in the thin-lens approximation the deflection of the pion in the magnetic field is equal to $\Delta\theta = \frac{x}{R}$ where R is the radius of curvature that can be calculated comparing the Lorentz force to the centrifugal force, then $\Delta\theta = \frac{x}{R} = \frac{qxB}{mv} = \frac{qxB}{p}$. Being the magnetic field equal to $B = \frac{\mu_0 I}{2\pi r}$, recalling that the surface is a paraboloid and then replacing $x = ar^2$ we get

$$\Delta\theta = \theta_{in} - \theta_{out} = \frac{r}{l} - \theta_{out} = \frac{\mu_0 I a r}{2\pi p} \propto r.$$

A point situated at a distance $l = f$ is focused if $\theta_{out} = 0$. f is then the focal length of the horn. Thus a pion generated in the target at a distance l entering the horn with an angle θ_{in} is focused if $\theta_{out} = 0$ or if

$$\frac{r}{f} = \frac{\mu_0 I a r}{2\pi p} \Rightarrow f = \frac{\pi}{\mu_0 a I} p.$$

Therefore, for every pion generated at a distance f, all the pions whose momentum equals $p = \frac{\mu_0 a I f}{\pi}$ are focused regardless of θ_{in}.

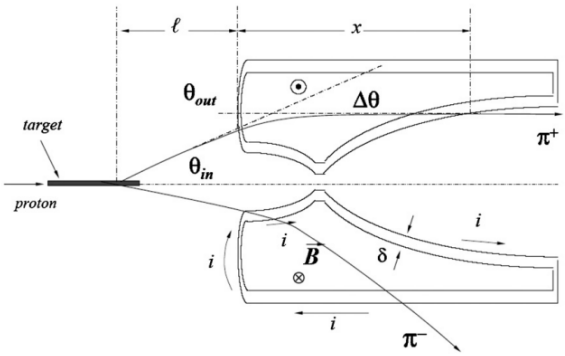

2.2.3 The near detector

The primary role of the DUNE near detector system is to characterize the energy spectrum and the composition of the neutrino beam at the source, in terms of both muon-flavoured and electron-flavoured neutrinos and antineutrinos, and to provide measurements of neutrino interaction cross sections.

The separation between fluxes of neutrinos and antineutrinos requires a magnetized neutrino detector to discriminate e^- from e^+ and μ^+ from μ^- produced in the neutrino charge-current interactions.

The reference design for the near detector design is the NOMAD-inspired fine-grained tracker (FGT).

2.3 Far site facilities

LBNF/DUNE at SURF includes facilities both on the surface and underground. A cryogenics infrastructure will support the far detector, divided into four 10 kt fiducial mass detector modules, two each in two caverns that will be carved to depth of 1.6 km and to a distance of 1300 km from the neutrino beam source.

2.3.1 The far detector

The far detector will be composed of four similar modules, each containing a liquid argon time-projection chamber (LArTPC) encapsulated by a cryostat. The LArTPC is a continuously sensitive detector that provides excellent tracking and calorimetry performance. It is ideal for massive neutrino detectors (such as the DUNE far detector) which require high signal efficiency and effective background discrimination, an excellent capability to identify and measure neutrino events over a wide range of energies, and high resolution in the reconstruction of kinematical properties. The detector will have a fiducial mass of 40 kt, a mass large enough to allow the collection of sufficient statistics for precise studies.

LArTPC working

A liquid Argon time-projection chamber consists in a liquid argon filled volume in an electric field. On passing through the detector, a particle will produce primary ionization creating an excited diatomic argon molecule. The electron released drifts toward the anode. Here there are three wire planes rotated by 60 degrees relative to one another and separated by a small gap. The last plane is called the collection plane; drift electrons are collected on these wires producing proportional signals used for calorimetric measurements. The three planes with different orientations allow the two dimensional trajectory reconstruction, while from electron drift times it is possible to reconstruct the track in three dimensions.

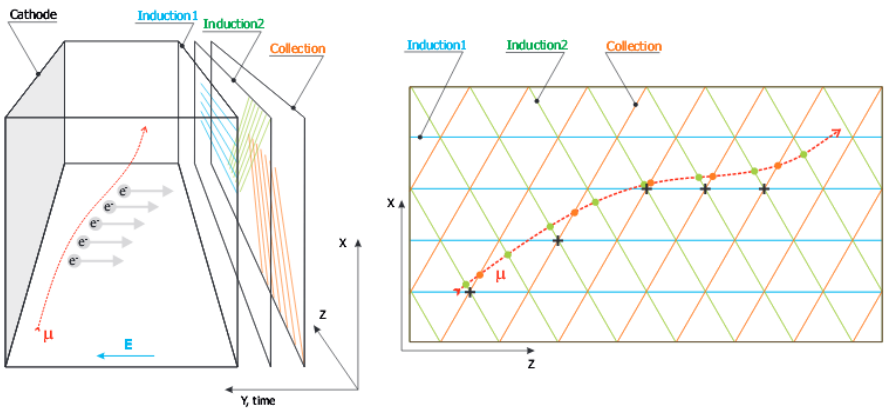

Chapter 3

Neutrino oscillations

3.1 Massive neutrinos and PMNS mixing matrix

The possibility of neutrino oscillations had been discussed since neutrinos were first discovered experimentally in 1956 but it was only around the end of the last century that the theory was validated: in 1998 Takaaki Kajita of the Super-Kamiokande Collaboration presented data showing the disappearance of atmospheric muon-neutrinos, as they travel from their point of origin to the detector. In 2002 the Sudbury Neutrino Observatory (SNO) Collaboration published evidence for conversion of electron-type neutrinos from the Sun into neutrinos of other flavours. The discovery of neutrino oscillations represents experimental evidence for the incompleteness of the Standard Model as a description of nature.

The fact that neutrinos can convert from one flavour to another, hence having nonzero masses, implies that the neutrino flavour states are not mass eigenstates but superpositions of such states, as it was first predicted by Pontecorvo in 1957 in analogy with neutral kaon mixing.

A neutrino is created in weak process in a certain flavour eigenstate. As the neutrino propagates through space, the quantum mechanical phases of the three mass states advance at different rates due to slight differences between the three mass eigenvalues. The mixture of mass states changes giving rise to a different mixture of flavour states. The relation between mass and flavour eigenstates can be expressed as the unitary transformation

$$|\nu_\alpha\rangle = \sum_i U^\dagger_{\alpha i}|\nu_i\rangle$$
$$|\nu_i\rangle = \sum_\alpha U_{\alpha i}|\nu_\alpha\rangle$$

where $i = 1, 2, 3$ and $\alpha = e, \mu, \tau$. $U_{\alpha i}$ represents the Pontecorvo–Maki–Nakagawa–Sakata (PMNS) matrix.

Parameters counting Be $|\nu_\alpha\rangle$ a neutrino state in the flavour basis, and $|\nu_i\rangle$ the same state in the mass basis, P and D unitary diagonal $N \times N$ matrices.

$$1 = \langle\nu_\alpha|\nu_\alpha\rangle = \langle\nu_\alpha|U^\dagger_{\alpha i}|\nu_i\rangle = \langle\nu_\beta|Q^{-1}_{\beta\delta}Q_{\delta\alpha}U^\dagger_{\alpha i}P^{-1}_{ij}P_{jk}|\nu_k\rangle = \langle\nu'_\alpha|U'^\dagger_{\alpha i}|\nu'_i\rangle$$

$|\nu'_\alpha\rangle$ and $|\nu'_i\rangle$ are still states respectively in the flavour and in the mass base. Old orthonormal basis-eigenvectors have been only multiplied by a phase. Thus one can redefine $U'^\dagger = QU^\dagger P^{-1}$ as the PMNS matrix. P contains N phases that can be chosen, for example, to remove all the phases from the first row of matrix $U^\dagger P^{-1}$. Q contains $N-1$ phases that can be chosen, for example, to remove all the phases from the first column of the matrix $U'^\dagger = QU^\dagger P^{-1}$. One phase has to be null to not add again phases to the first row. Therefore, $U'^\dagger$ has

$$2N^2 - \underbrace{N^2}_{\text{from unitarity}} - \underbrace{(2N-1)}_{\text{unphys. phases}} = (N-1)^2$$

parameters, thus 4 parameters if U is a 3×3 matrix.

A 3×3 unitary matrix with 4 parameters (3 angles and a phase) can be decomposed in the following way.

$$U^\dagger = \begin{pmatrix} U_{e1} & U_{e2} & U_{e3} \\ U_{\mu 1} & U_{\mu 2} & U_{\mu 3} \\ U_{\tau 1} & U_{\tau 2} & U_{\tau 3} \end{pmatrix} = \begin{pmatrix} 1 & 0 & 0 \\ 0 & c_{23} & s_{23} \\ 0 & -s_{23} & c_{23} \end{pmatrix} \begin{pmatrix} c_{13} & 0 & s_{13}e^{i\delta} \\ 0 & 1 & 0 \\ -s_{13}e^{-i\delta} & 0 & c_{13} \end{pmatrix} \begin{pmatrix} c_{12} & s_{12} & 0 \\ -s_{12} & c_{12} & 0 \\ 0 & 0 & 1 \end{pmatrix}$$
$$= \begin{pmatrix} c_{13}c_{12} & c_{13}s_{12} & s_{13}e^{-i\delta} \\ -s_{12}c_{23} - c_{12}s_{23}s_{13}e^{i\delta} & c_{12}c_{23} - s_{12}s_{23}s_{13}e^{i\delta} & s_{23}c_{13} \\ s_{12}s_{23} - c_{12}c_{23}s_{13}e^{i\delta} & -c_{12}s_{23} - s_{12}c_{23}s_{13}e^{i\delta} & c_{23}c_{13} \end{pmatrix}$$

where $s_{13} = \sin(\theta_{13})$ etc., θ_{13}, θ_{12} and θ_{23} are neutrino mixing angles and δ_{CP} the CP violating phase. Two more phases are needed if neutrinos are Majorana particles.

If $U_{\alpha i}$ were proved by experiments not to be unitary, a sterile neutrino or some other new physics would be required.

Flavour conversion probability $|\nu_i\rangle$ is an eigenstate of the free hamiltonian, therefore it can be written as $|\nu_i(t)\rangle = e^{-i(E_i t - \vec{p}_i \cdot \vec{x})}|\nu_i(0)\rangle$ with $\vec{p}_i^2 \simeq E_i^2$. The transition probability can thus be expressed in terms of mixing angles, square mass differences $\Delta m_{ij}^2 = m_i^2 - m_j^2$, the CP phase and the neutrino energy.

$$P_{\alpha\to\beta} = |\langle\nu_\beta(t)|\nu_\alpha\rangle|^2 = |\sum_k U_{\alpha k}^\dagger e^{-iE_k t} U_{\beta k}|^2 = \sum_{k,j} U_{\alpha k}^* U_{\beta k} U_{\alpha j} U_{\beta j}^* e^{-i(E_k - E_j)t}$$

In the standard theory of neutrino oscillations it is assumed that all massive neutrinos have the same momentum $\vec{p}_i \simeq \vec{p}$. Since detectable neutrinos are ultrarelativistic $E_i \simeq |\vec{p}_i| \approx |\vec{p}| \equiv p = E$, with E the energy of neutrino in the massless approximation. Therefore

$$E_i = \sqrt{\vec{p}_i^2 + m_i^2} \simeq p_i + \frac{m_i^2}{2E_i} \simeq E + \frac{m_k^2}{2E} \Rightarrow E_i - E_k = \frac{m_i^2 - m_k^2}{2E} = \frac{m_{ik}^2}{2E}$$

In the ultrarelativistic approximation $t \sim L$ (natural units), leading to

$$\begin{aligned} P_{\alpha\to\beta} &= \sum_{i,j} U_{\alpha i}^* U_{\beta i} U_{\alpha j} U_{\beta j}^* e^{-i\frac{\Delta m_{ij}^2 L}{2E}} \\ &= \delta_{\alpha\beta} - 4\sum_{i>j} \Re(U_{\alpha i}^* U_{\beta i} U_{\alpha j} U_{\beta j}^*) \sin^2\left(\frac{\Delta m_{ik}^2 L}{4E}\right) + 2\sum_{i>j} \Im(U_{\alpha i}^* U_{\beta i} U_{\alpha j} U_{\beta j}^* \sin\left(\frac{\Delta m_{ik}^2 L}{2E}\right) \end{aligned}$$

Restoring the c and $\hbar$

$$\frac{1}{\hbar}\frac{\Delta m_{ik}^2 c^4}{4E}\frac{L}{c} = 1.27\frac{\Delta m_{ik}^2 L}{E}\frac{[\text{GeV}][\text{eV}]^2}{[\text{Km}]}$$

Two neutrino case The above formula is correct for any number of neutrino flavours involved. Writing it explicitly, one may get stuck in an extremly long formula if there are more than two neutrinos involved. Anyway, there are several cases in which only two neutrino flavours take part significantly in the oscillation. For example, $\nu_\mu \to \nu_\tau$ in the atmospheric mixing or $\nu_e \to \nu_x$ in the solar case, where $|\nu_x\rangle$ is a superposition of $|\nu_\mu\rangle$ and $|\nu_\tau\rangle$. In these cases, the PMNS mixing matrix simplifies to a 2-dimensional rotation. Consider the atmospheric case. Since $U_{\alpha i}$ has only real elements, the transition probability is given by

$$\begin{aligned} P_{\mu\to\tau} &= -4U_{\mu 2}U_{\tau 2}U_{\mu 1}U_{\tau 1}\sin^2\left(\frac{\Delta m_{23}^2 L}{4E}\right) \\ &= 4\sin^2(\theta_{23})\cos^2(\theta_{23})\sin^2\left(\frac{\Delta m_{23}^2 L}{4E}\right) \\ &= \sin^2(2\theta_{23})\sin^2\left(1.27\frac{\Delta m_{23}^2 L}{E}\frac{[\text{GeV}][\text{eV}]^2}{[\text{Km}]}\right). \end{aligned}$$

Since the majority of neutrinos produced in LBNF will be ν_μ from the π^+ decay ($\pi^+ \to \mu^+ + \nu_\mu$)[1] the previous formula can be used to estimate the energy at which the maxima of oscillation are expected at DUNE far detector.

$$E_n = \cdot 1.27 \cdot 1300 \cdot \Delta m_{23}^2 \frac{2}{(2n+1)\pi} = \cdot 1.27 \cdot 1300 \cdot 2.44 \cdot 10^{-3}\frac{2}{(2n+1)\pi} \to E_0 = 2.56\text{GeV}, E_1 = 0.85\text{GeV}, ...$$

The following graph was made using OscCalculator, the program implemented in the LBNF code to evaluate the oscillation probability in the 3 flavour hypothesis.

Because of the low $\nu_\mu \to \nu_e$ transition probability, one can notice that the two neutrino model is a good approximation of the three neutrino model. It can also be noticed that the $\nu_\mu \to \nu_\tau$ transition is not very sensible to the CP violation phase.

[1]The near detector flux is composed mainly by ν_μ and partially by ν_e from the decay of μ^+ and by $\bar{\nu}_\mu$ from the ν^+ decay and from π^- decay coming from the K^+ decay. In antineutrino mode the situation is reversed. It is not implemented in the simulations the possibility of ν_τ from D_s decay. All ν_τ comes from oscillations

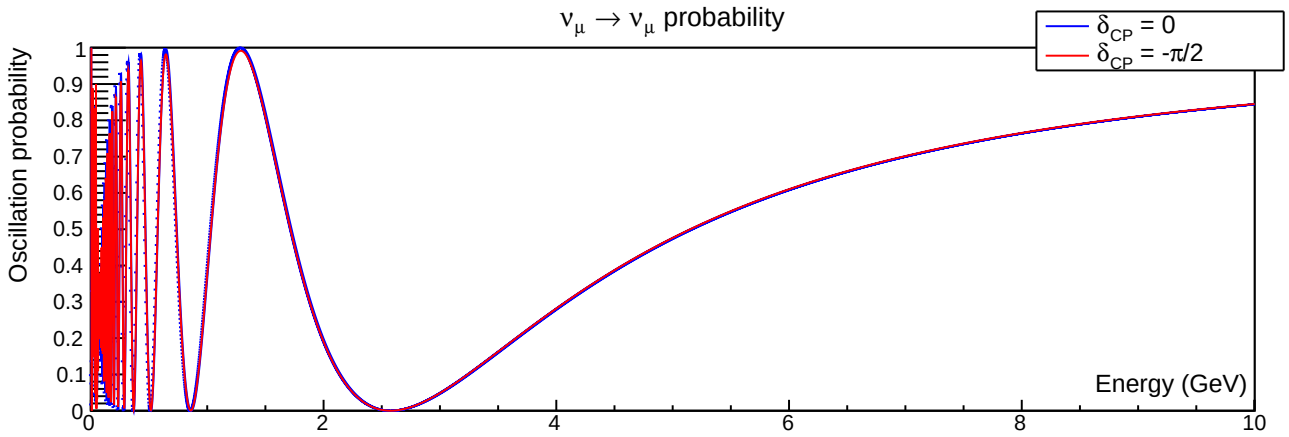
$\nu_\mu \rightarrow \nu_\mu$ probability
$\delta_{CP} = 0$
$\delta_{CP} = -\pi/2$
Oscillation probability
Energy (GeV)

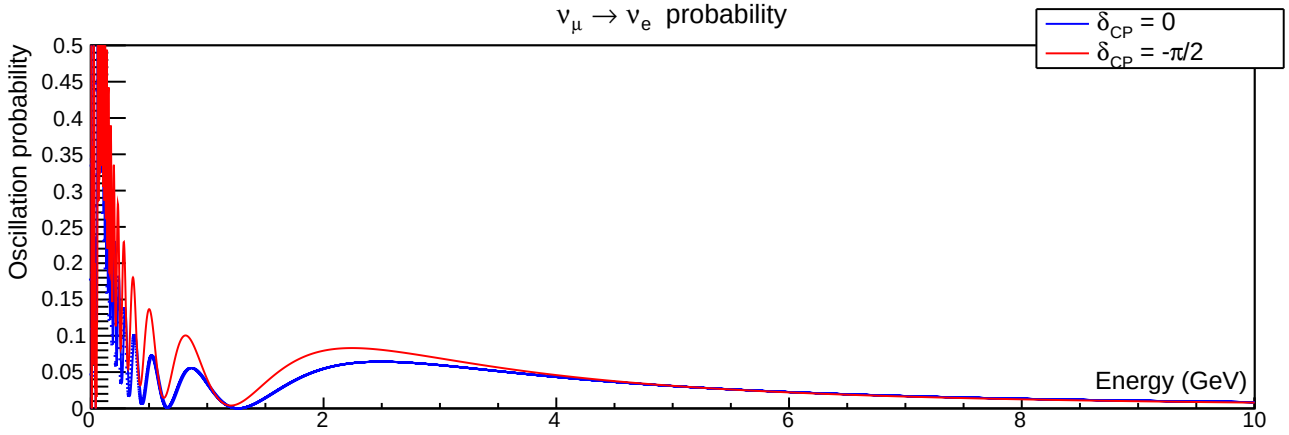
$\nu_\mu \rightarrow \nu_e$ probability
$\delta_{CP} = 0$
$\delta_{CP} = -\pi/2$
Oscillation probability
Energy (GeV)

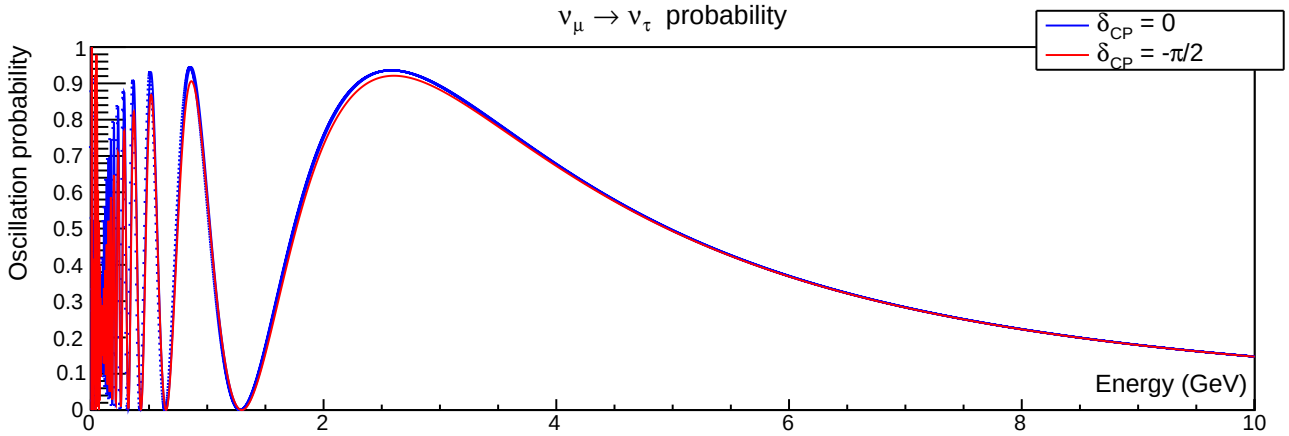
$\nu_\mu \rightarrow \nu_\tau$ probability
$\delta_{CP} = 0$
$\delta_{CP} = -\pi/2$
Oscillation probability
Energy (GeV)

Chapter 4

Neutrino detection

The ν_τ probability to detect a ν_τ event at the far detector is proportional to

1. the oscillation probability,
2. the charge-current ν_τ cross section,
3. reconstruction efficiency of LArTPC detector.

ν_τ CC cross-section The following cross-section graph is made with cross-section data coming from GENIE Neutrino Monte Carlo Generator included into the LBNF code.

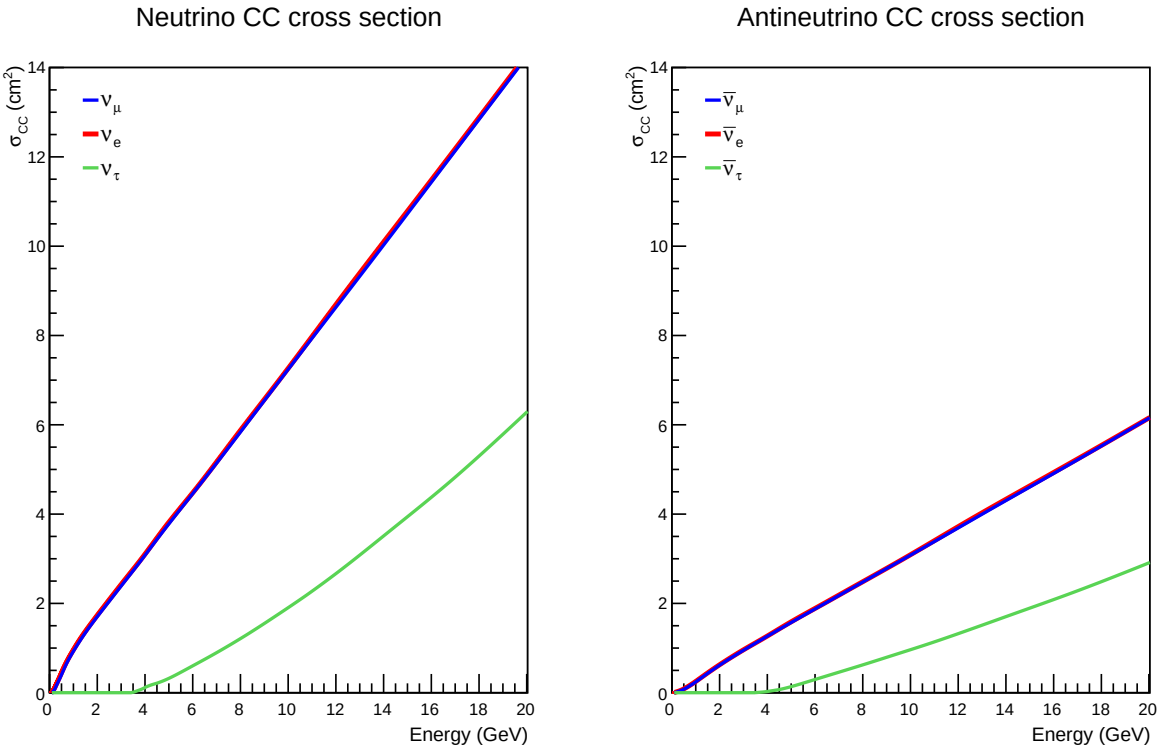

The $\bar{\nu}$ CC cross-section is about half the ν CC cross-section. This implies that the background is higher when running in antineutrino mode (horns focusing negative-charged particles) than in neutrino mode (horns focusing positive-charged particles).

The ν_τ CC cross-section has a threshold at 3.5GeV, that is the minimum neutrino energy required to produce a τ in a CC interaction. Consider $\nu_\tau + n \to \tau^- + p$, be $p^2 = (M_n + E)^2 - E^2$ the total squared four-momentum in the initial state in the neutron rest frame and $q^2 = (m_\tau + M_p)^2$ the total squared four-momentum in the final state in the threshold condition in the MC rest frame. E is the neutrino energy, $M_n \approx M_p \simeq 939$ MeV the neutron mass and $m_\tau \simeq 1776$MeV. p^2 is a Lorentz-invariant conserved quantity, thus

$$p^2 = q^2 \Rightarrow E_{\nu\ \mathrm{min}} \simeq \frac{m_\tau^2 + 2M_n m_\tau}{2M_n} = 3.5\mathrm{GeV}$$

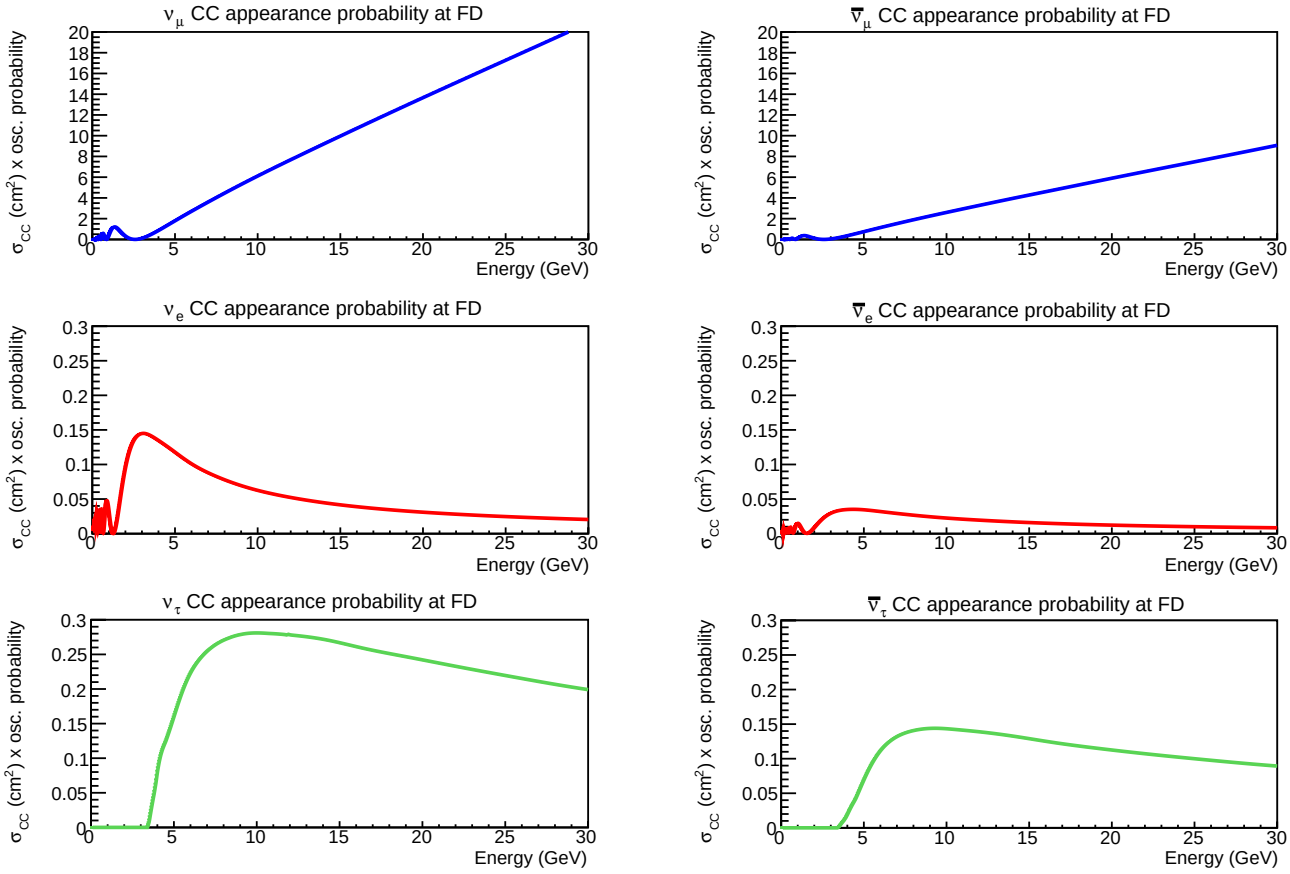

ν_τ recognition All neutral-current interactions are considered as background, since there is no way to understand the interacting neutrino flavour.

The search for ν_τ CC interactions is performed by identifying the τ decays. Neutrino interactions are selected by requiring the presence of at least one track in addition to the τ decay products such that the two tracks have a common vertex inside the detector volume. DUNE LArTPC detector does not have enough resolution to see the τ vertex, nevertheless the τ can be discriminated using the same kinematical criteria that have been used in NOMAD experiment.

A τ lepton may experience a lepton decay or a hadron decay. In both cases the track created by τ decay products is well discernible and isolated in comparison to the hadronic jet. This difference can be quantified by introducing the variable Q_T defined as the component of the visible τ decay products momentum perpendicular to the total visible momentum of the event.

In neutral-current events a particle belonging to the hadronic jet could be confused with a τ decay product, but a small value of Q_T would be measured, while τ decays have larger Q_T values. After fixing a threshold of acceptance, one can easily distinguish a ν_τ event in which τ undergoes hadronic decay from the neutral-current background.

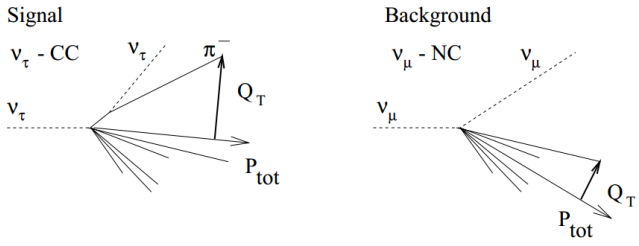

To distinguish ν_τ CC events in which τ undergoes a leptonic decay from their background (CC ν_e and ν_μ events), we can introduce the quantity $\not{p}_T = |\vec{p}_T^{\,h} - \vec{p}_T^{\,l}|$ where $\vec{p}_T^{\,h}$ and $\vec{p}_T^{\,l}$ are respectively the projection of the hadron jet momentum vector and of the lepton (e, μ) momentum vector on the plane transverse to the beam. If the missing transverse momentum $\not{p}_T$ is large, it means that something we don't see is carrying the missing transverse momentum. Thus, the observed event is a CC ν_τ event and $\not{p}_T$ is carried by the couple $\bar{\nu}_l, \nu_\tau$ of neutrinos produced in the τ decay ($\tau \to l + \bar{\nu}_l + \nu_\tau$ with $l = e, \mu$). In CC ν_e and ν_μ events, $\not{p}_T$ should be zero. Actually, $\not{p}_T$ it is not zero due to due to measurement errors, losses of neutral hadronic particles and nuclear

effects, but it is smaller than it is for ν_τ CC events. Again, after fixing a threshold of acceptance, one can easily distinguish a ν_τ event in which τ undergoes leptonic decay from the charged-current background.

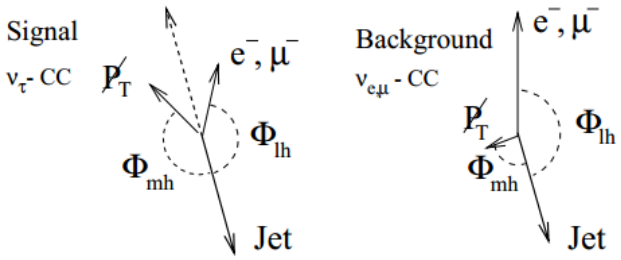

Reconstruction efficiency To estimate the reconstruction efficiency of DUNE LArTPC it is would be necessary to simulate a big number of events and to evaluate for each event the kinematical variables Q_T and $\not{p}_T$. Then it would be possible, for every τ decay channel and its relative background, to analyse the distribution of the kinematical variables and to set a threshold that allows to separate with a certain confidence the ν_τ events from the background. The threshold has to be chosen so that the likelihood-ratio (probability of a ν_τ interaction to be recognised as a ν_τ interaction divided by the probability of an event from background to be recognised ν_τ interaction) is high enough. All the ν_τ decay channels that can be reconstructed by the detector and their relative branching ratio are mentioned in the table below.

decay channel	branching ratio
$\tau \to \nu^- \quad \bar{\nu}_\mu \quad \nu_e$	17.4%
$\tau \to e^- \quad \bar{\nu}_e \quad \nu_e$	17.8%
$\tau \to \pi^- \quad \nu_\tau$	10.8 %
$\tau \to \pi^- \quad \pi^0 \quad \nu_\tau$	25.5%
$\tau \to 3\pi(\pi^0)$	15.2%
total	86.7 %

The reconstruction efficiency of DUNE LArTPC has not been simulated and calculated yet, but it should range between 10% and 30%.

Chapter 5

G4LBNE software

The software is maintained in a git repository that can be cloned also without authentication. All the information about how to download, install, build and run G4LBNE can be found at the URL https://cdcvs.fnal.gov/redmine/projects/lbne-beamsim/wiki/Wiki. Briefly, the simulations are performed by following the steps listed below.

- First, one has to create a macro containing
  - all the commands to modify the geometry of the beam-line from the default one,
  - the command /LBNE/det/construct that tells G4LBNF to build the geometry,
  - commands for enable the 3D visualization, if needed
  - the command /run/initialize,
  - information about the proton momentum and the number of protons on target,
  - the command /run/beamOn to start the simulation.
- then one can run the macro locally or submit it to the grid.
- In the former case, when the submitted job starts, G4LBNF is called.
  - G4LBNF reads the geometry and checks for overlaps of the volumes,
  - loads the reference physics list containing all the physical processes to be simulated,
  - configures the proton beam,
  - initializes the random number generator,
  - runs the chosen number of protons. G4LBNF transports every primary proton step by step evaluating for every step where it is, its energy and its interaction probability. Then it performs the same simulations for every daughter particle. If a particle exits the mother volume[1] or has no chance to decay in a neutrino, then the track is not to be stored.
  - In the end, G4LBNF stores all the information about neutrinos produced inside the mother volume in an ntuple. All the physical properties of every neutrino (neutrino energy, neutrino vertex and momentum, neutrino parent vertex and momentum, parent type, importance weight etc.) are related to a branch of the ntuple[2].
- eventsRate.C is called and reads the ntuple.
  - To make the simulation faster it is supposed that all neutrinos arrive in the far detector and a weight is applied a posteriori to take into account the probability of every neutrino to actually reach the far detector.
  - eventsRate.C performs relativistic calculations and reads importance weight and detector weights from the ntuple to evaluate the total weight,
  - fills the unoscillated flux histograms for every neutrino or antineutrino type at near and far detector.
  - multiplies the total weight by CC or NC cross section (generated by GENIE) of every neutrino or antineutrino type and fills the unoscillated events rate histograms at near and far detector.
  - eventsRate.C calls OscCalculator.C and evaluates for every neutrino the probability of oscillate into another flavour at the far detector,
  - fills the oscillated flux histograms the oscillated events rate histograms at near and far detector for every neutrino and antineutrino type.

[1] Biggest volume which contains every other volume.

[2] The documentation on the ntuple branches can be find here: https://cdcvs.fnal.gov/redmine/projects/lbne-beamsim/wiki/Ntuple

5.1 Issues with oscillated ν_τ CC events rate histograms

In the first simulation trial, the events rate histogram for oscillated ν_τ at far detector appeared to be incorrect due to the fact that there was a non-zero events rate in correspondence of neutrinos with energy below 3.5 GeV.

Reading the code, came out that

- eventsRate.C only knew ν_μ, $\bar{\nu}_\mu$, ν_e and $\bar{\nu}_e$ cross sections and was reading the ν_μ cross section (default choice) to build the CC events rate histogram for oscillated ν_τ.
- The multiplication of the weight by the cross section necessary to fill the events rate histograms was performed before the neutrino was oscillated. Therefore, the appearance probability of ν_τ (equal to weight $\times$ cross section) was proportional to ν_μ cross section or to ν_e cross section depending on the neutrino flavour before oscillation instead of being proportional to ν_τ cross section.

After eliminating the issues mentioned above, the events rate histograms for oscillated ν_τ and $\bar{\nu}_\tau$ appeared to be correct and I was able to start moving the target and run the macros.

Chapter 6

Results of simulations

6.1 Optimized and default reference designs

First, I ran two simulations to see how many ν_τ CC events I could get with the default reference design and with the optimized design.

The *zero* point along the z axis is located approx at the beginning of the first horn. Settings for the default reference design are the following:

- the target[1] is 954 mm long,
- the z offset of the target is -464 mm, so it is partially inside horn 1,
- horn 1 is 3.5 m long,
- the z offset of horn 2 is 6.5 m,
- horn 2 is 4.2 m long.

Using the default reference design, 225 ν_τ events per 40 kt per year should appear with an error on the mean of 3 events.

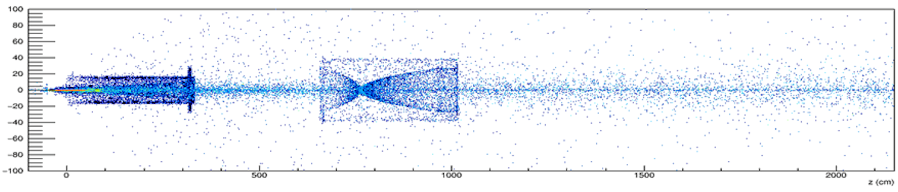

Figure 6.1: Parent production vertex plot for the default reference design

Using the optimized design, 128 ν_τ events per 40 kt per year should appear with an error on the mean of 1 event. The number of events is roughly half of what can be obtained with the reference design; this shows why for ν_τ appearance it is better to start from the reference design.

An alternative idea for the ν_τ appearance configuration would be to replace the optimized horn A and B with a NuMI-style horn 1 and to leave the optimized horn C at the end of low-energy experiments, bypassing the expansive construction of the NuMI-style horn 2. However, as will be seen later, extending radially horn 2 significantly reduces the events rate. This means that it is necessary to use a radially small horn 2 to get good results. This is the reason why a simulation using a NuMI-style horn 1 together with the optimized horn C was not made.

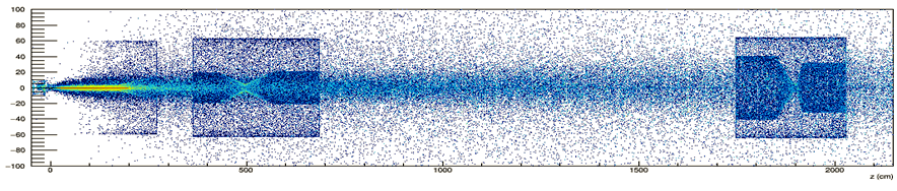

Figure 6.2: Parent production vertex plot for the optimized design

[1] In the default reference design a NuMI style graphite target is used. See detailed description in the next section.

6.2 Placing the target and the second horn

Starting from the default reference design, I began to increase the distance between the target and horn 1 and to turn away horn 2 from horn 1.

The z-offset of the target ranges between 60 cm and 480 cm with a step of 30 cm, while the z-offset of horn 2 ranges between 6.5 m (default reference design) and 17.5 m (the maximum distance allowed by the size of the target hall) with a step of 1 m.

To avoid overlaps, some volumes have not been installed in these simulations. In particular, I removed the baffle, the structure upstream of the target, the shield and the decay pipe snout.

The current flowing into the horns is 230 kA.

The target is the default NuMI style target. It is composed by 47 graphite segments, each 2 cm long and 10 mm width, spaced 0.2 mm apart. The target is cooled above and below by a titanium tube filled with water.

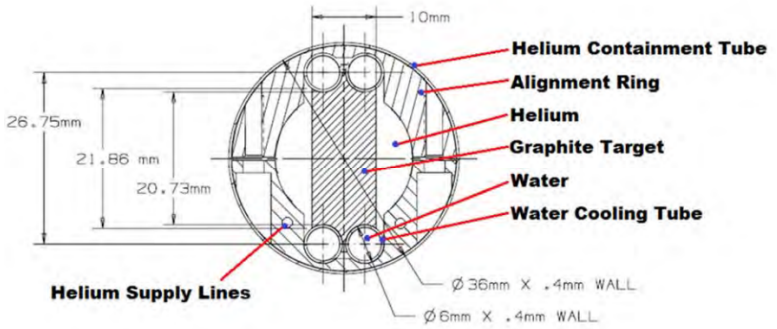

Figure 6.3: NuMI target

The beam is composed by protons of 120 GeV fast-extracted from the Main Injector. The beam power is 1.2 MW. The beam sigma is 1.7 mm in both X and Y coordinates; this is the default value chosen so that the 99.97% of the beam goes into the NuMI target.

I ran 100 simulations each with 100000 protons on target for each configuration. The number in each box is the mean of the 100 simulations. The mean absolute error ranges from 1 (blue boxes) to 5 (dark red boxes) events.

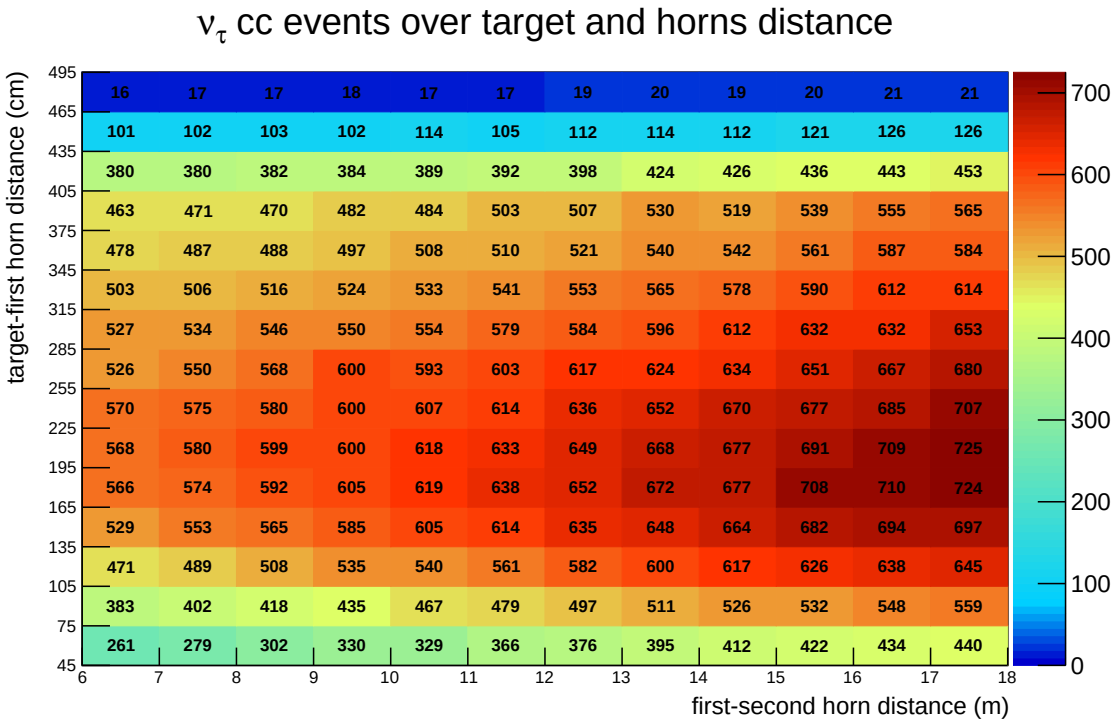

The plot shows that horn 2 has to be placed as far as possible from horn 1 while the target needs to be placed about at $z = -2m$.

The following two plots were made to better understand where to place the target. The second horn's z-offset is set at 17.5 m.

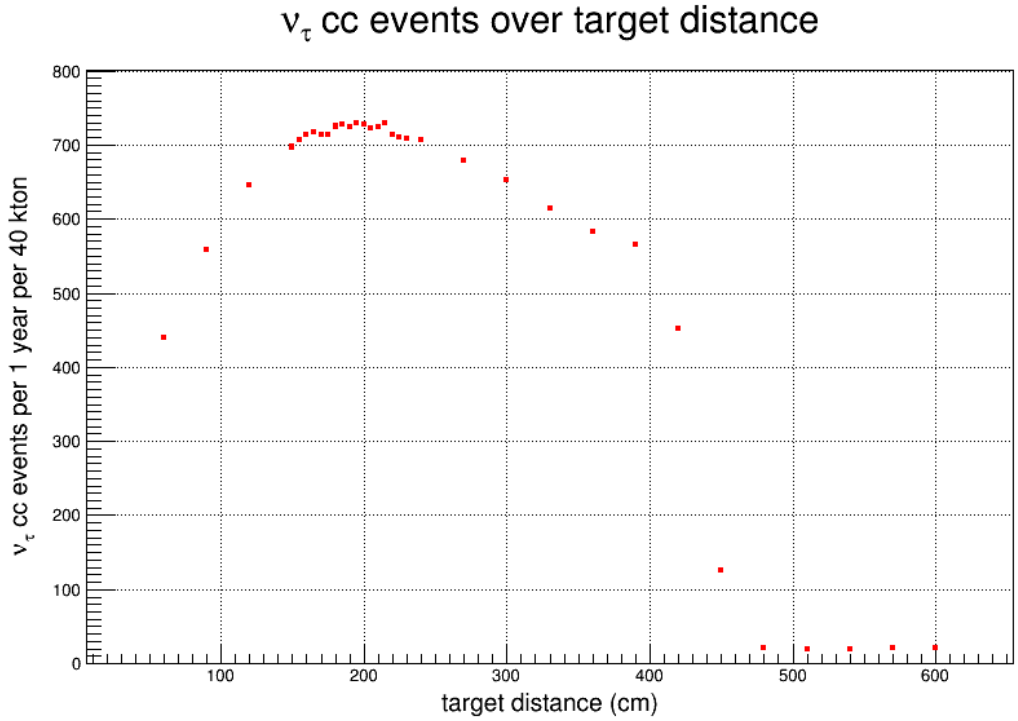

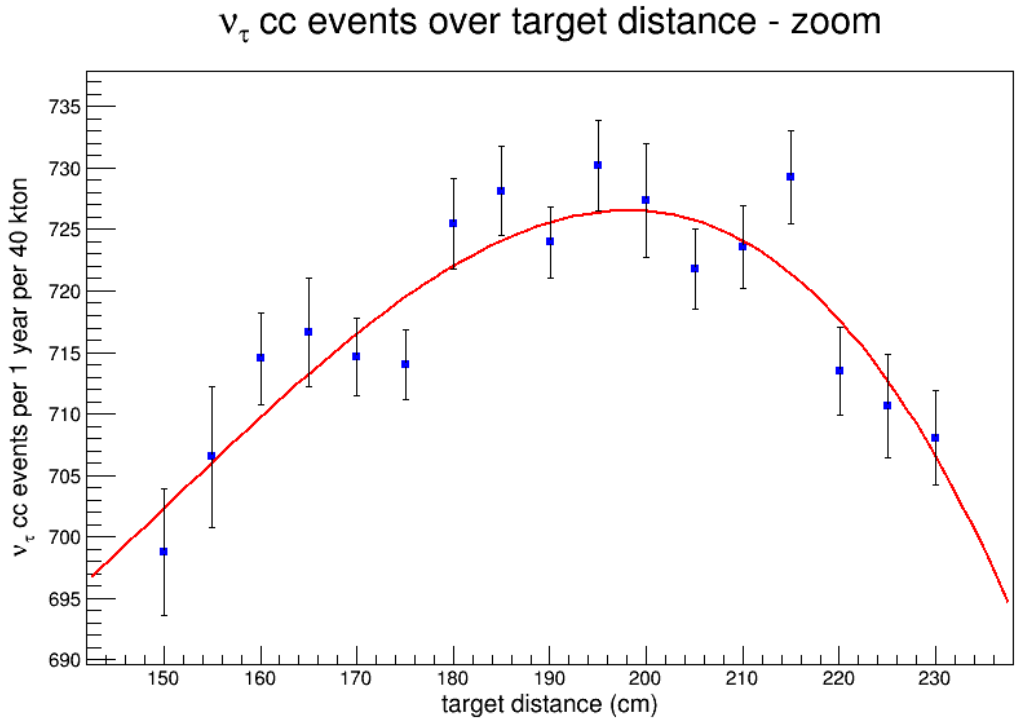

The red line represents the cubic function $f(x) = ax^3 + bx^2 + c^x + d$ that I used to fit the data. The curve has its maximum at 198 ± 4 cm, the error evaluated taking into account the fitted parameters a, b and c and their errors.

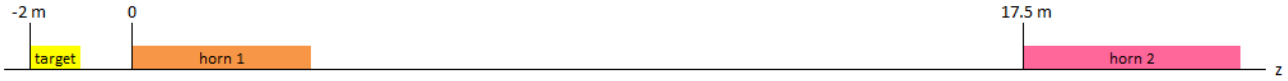

Figure 6.4: In-scale depiction of the configuration used in the further simulations

6.2.1 2013 vs. 2016 neutrino oscillation parameters

In the plot below, the red points represent the number of events from simulations made before updating the neutrino oscillation parameters to 2016, i.e with 2013 parameters. There is a little difference between 2013 and 2016 parameters but apparently nature worked in our favour; 10% more events appear using 2016 parameters instead of the older ones.

PDG 2013	**PDG 2016**
$\Delta m^2_{21} = 7,50 \cdot 10^{-5} eV^2$	$\Delta m^2_{21} = 7,53 \cdot 10^{-5} eV^2$
$\Delta m^2_{23} = 2,32 \cdot 10^{-3} eV^2$	$\Delta m^2_{23} = 2,44 \cdot 10^{-3} eV^2$
$\theta_{12} = 0,591$	$\theta_{12} = 0,584$
$\theta_{13} = 0,16$	$\theta_{13} = 0,1485$
$\theta_{23} = 0,785$	$\theta_{23} = 0,7994$

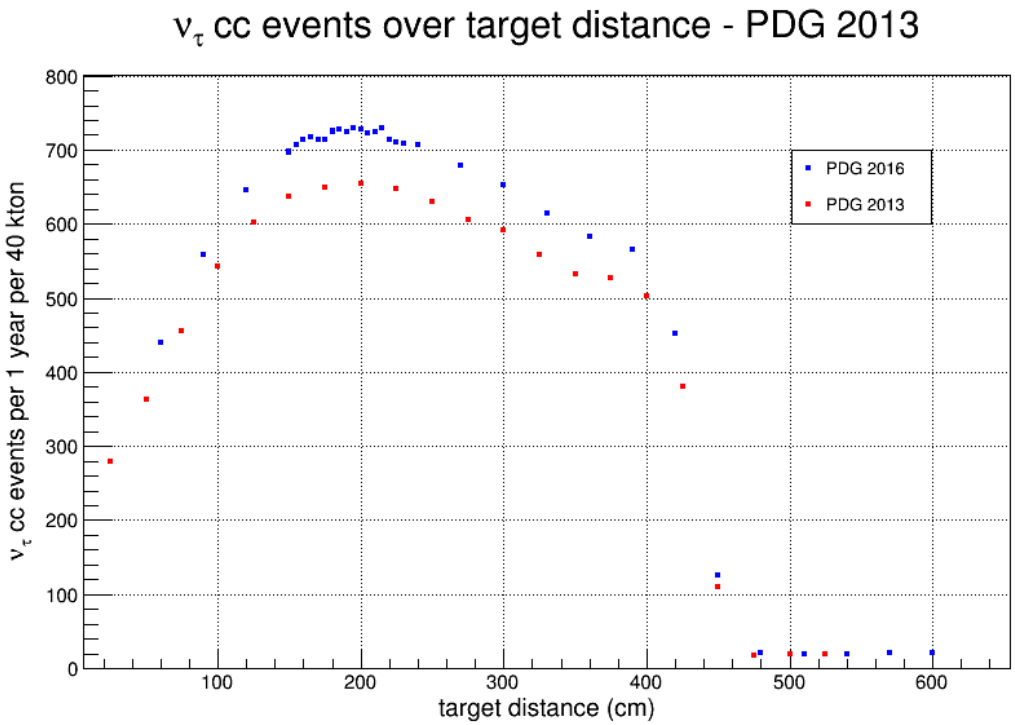

6.3 Rescaling the second horn

After moving the target and the second horn to the best configuration found before, I tried to radially and longitudinally rescale the second horn.

The settings (current and voltage of the horns, target type and beam configuration) are the same as in the previous section.

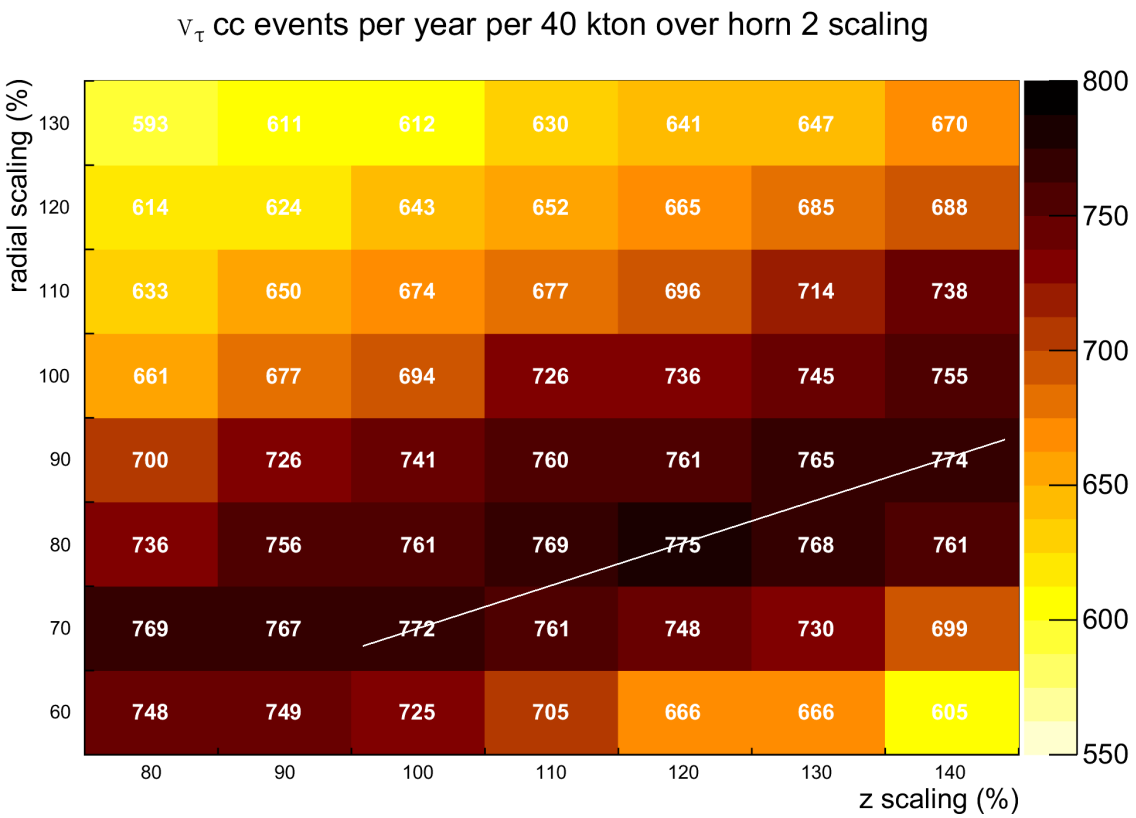

There appears a line of maxima all related to the same ratio.

In the macros I used to run these simulations I put the command RadialRescaleCst that was supposed to narrow the neck of horn 2 ensuring best focusing. I set RadialRescaleCst at 8 mm. However for a 100% radial and 100% longitudinal rescaling I got 694 events, i.e. 4.3% less than in the previous simulation. Since the standard error of the mean is 5 events for both the simulations, the two results were not consistent.

The command RadialRescaleCst was fixing the diameter of the neck making it larger than normal in the not-rescaled case, causing a loss of focusing and thus a loss of neutrino flux.

I removed the RadialRescaleCst command and I got the following result, where the not-rescaled case is consistent with the simulation made in the previous section. Here, for each point, the diameter of the second horn's neck is not fixed but radially rescaled as the rest of the horn.

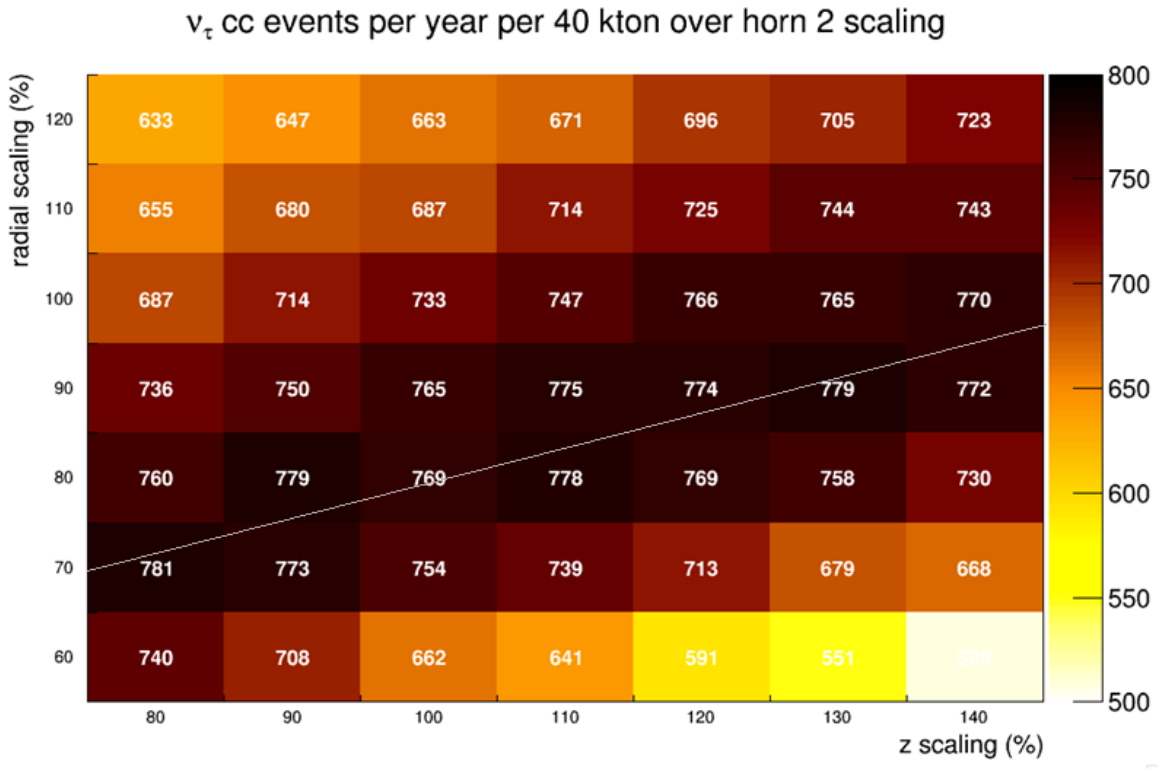

Again, the plot reveals a line of maxima.

One has to choose whether to shrink or to enlarge horn 2. Leaving aside considerations on the cost or possible engineering difficulties in the construction of a smaller horn, it would be better to shorten horn 2. In fact, considering the limited size of the target hall, this choice would give the chance to put horn 2 even further away from horn 1, gaining events.

In the further simulations I used horn 2 radially rescaled by 70% and longitudinally rescaled by 100%. This is not the best configuration but I was able to build the previous plot after running the simulations included in the next section. This does not change the validity of the results contained in the subsequent section, although slightly higher numbers could have been obtained[2].

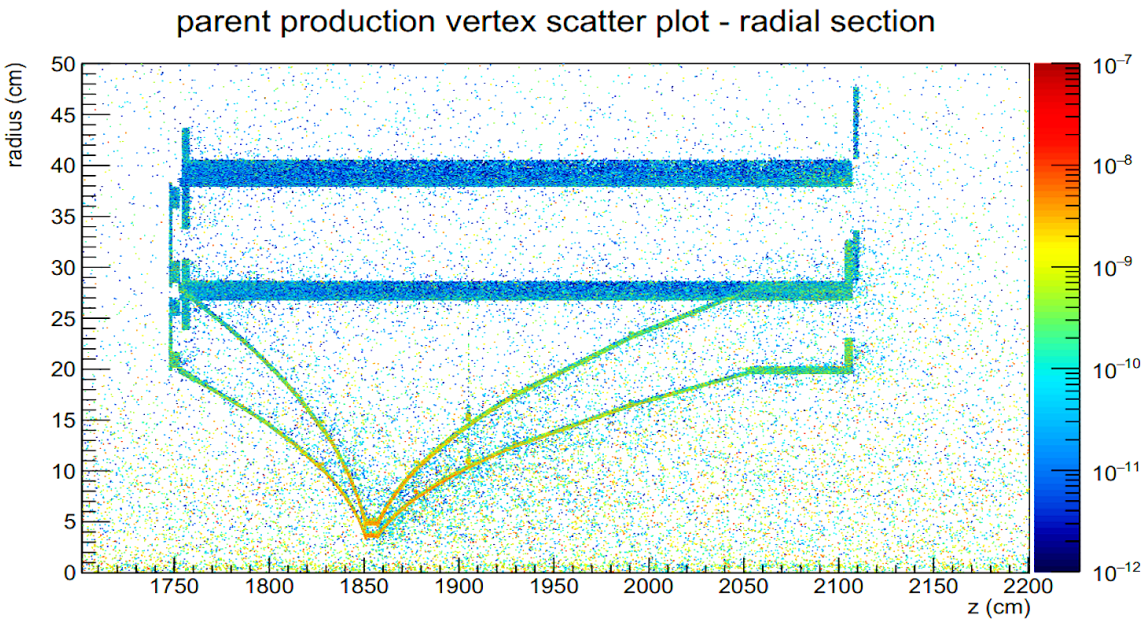

Figure 6.5: Standard horn 2 and 70% radially rescaled horn 2 superimposed

6.4 Modifying the target

The NuMI target could not be the best for a ν_τ appearance experiment, because of the probability of re-interactions. In addition, it would be better to use a longer target in order to reduce the number of neutrons that have not interacted and thus to deposit less energy on the absorber at the end of the decay pipe.

I first tried to lengthen the NuMI target to 2 m. Here horn 2 is not rescaled in order to compare the results with those of section 6.1.

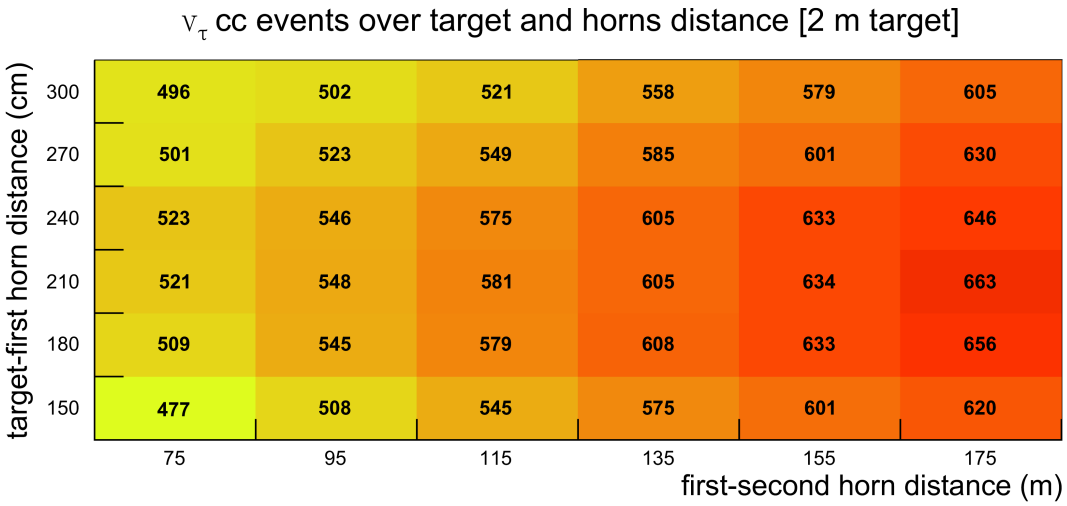

[2]The best configuration seems to be with horn 2 radially rescaled by 70%, longitudinally rescaled by 80% and placed at 18.3 m (as far as possible) from zero.

With the target at 2 m from the zero and horn 2 at the maximum distance the number of events decrease by 8.5%.

6.4.1 Multi spheres target

An alternative to the graphite NuMI target could be to use a helium cooled beryllium spherical array target (SAT). Spheres fit tightly inside a triple helix structure which provides correct location. This target has been designed for a future beam power upgrade; it may come in handy to the ν_τ appearance experiment because the existence of empty spaces inside the target would reduce the probability of re-interactions. I choose beryllium since from previous studies it appear to work better than graphite.

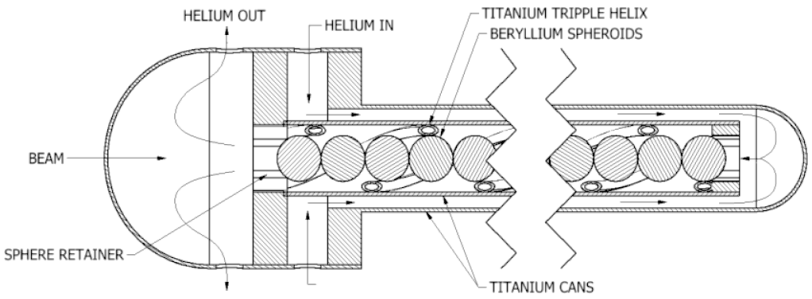

Two SAT designs were implemented in previous studies, using 13-mm or 17-mm-diameter spheres. I tried both the designs and the thinner array was found to generate more ν_τ CC events.

As a consequence of the previous result, I selected the 13-mm-diameter spheres target and I tried to modify the length of the target. The length shown on the plot is not the real length of the target, since this quantity is automatically rounded by the piece of code in which the multi spheres target is defined so that the array contains an integer number of spheres. All the settings are the same as in section 6.3 except that horn 2 is radially rescaled by 70% and the beam sigma (in both X and Y coordinates) is 1/3 the radius of the spheres, i.e. 2.16 mm for 13-mm-diameter spheres and 2.83 mm for 17-mm-diameter spheres.

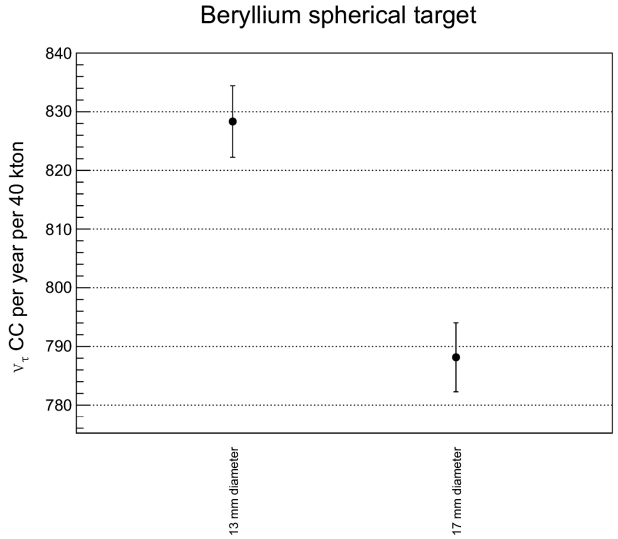

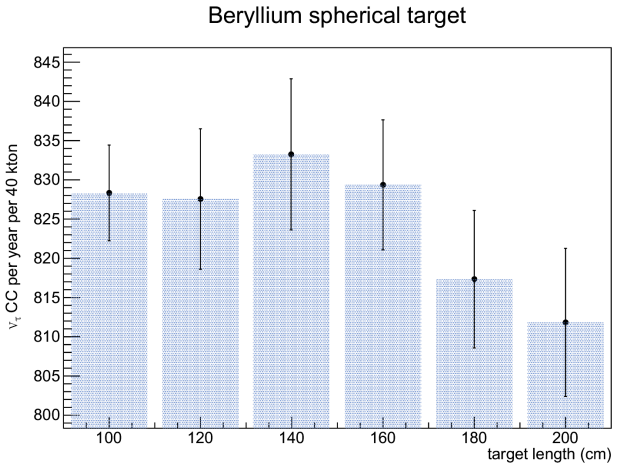

Here about 1.5% of CC events are lost by lengthen the target to 2 m. The good thing is that the target can be lengthen by 160% without losing events.

6.4.2 Cylindrical target

Another option could be to use a helium cooled simple cylindrical graphite target. Again this type of target reduces the probability or re-interactions because, there is not graphite above and below the circular area exposed to the beam, opposed to what happens to the NuMI target.

The settings are the same as those used for the beryllium spherical target, except for the target. Horn 2 is radially rescaled by 70%, not longitudinally rescaled an placed at 17.5 m from horn 1. The beam size is always set to be the target radius divided by 3.

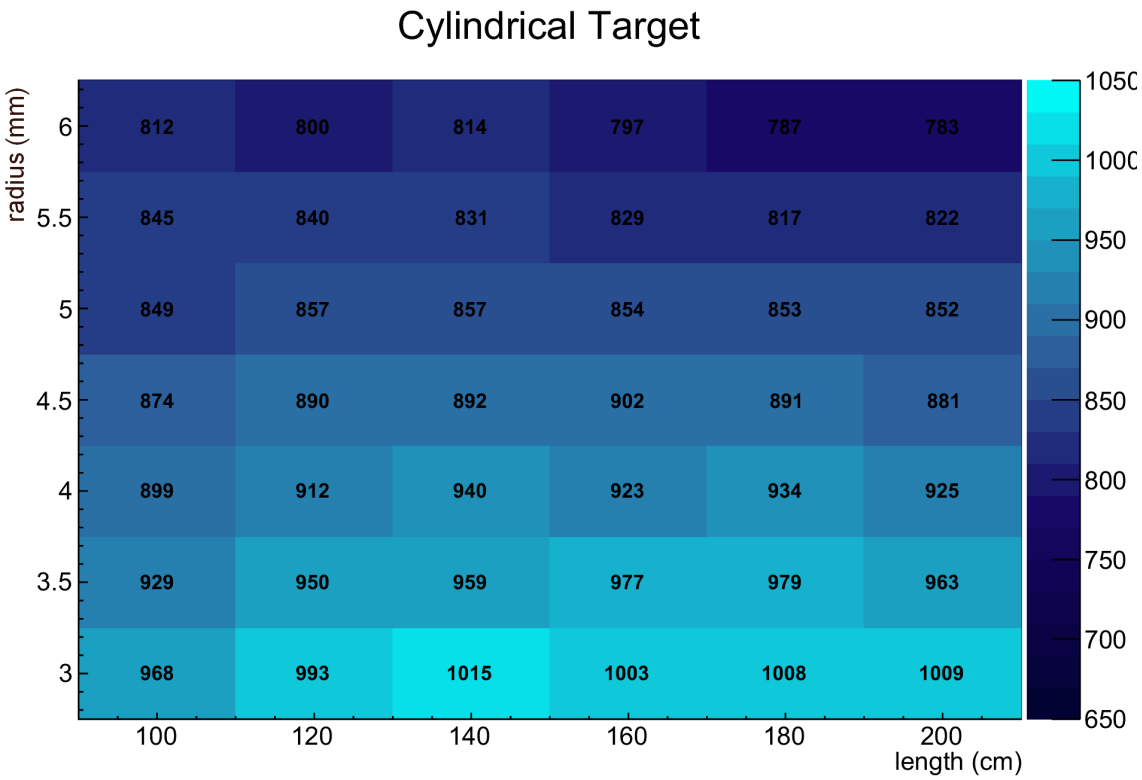

More events appear if the target is thinner. Moreover, choosing a small radius it seems to be possible to build a longer target without lowering the events rate, thus storing less energy in the absorber. On the contrary, choosing a large radius one would observe a lower events rate by making the target longer.

Nevertheless, a 3-mm-radius target would be surrealistic, since it would break if exposed to a 1.2-MW-beam.

Below, a scan of the oscillated ν_τ CC events rate over the target length for a 3-mm-radius cylindrical target and a more realistic 5-mm-radius cylindrical target.

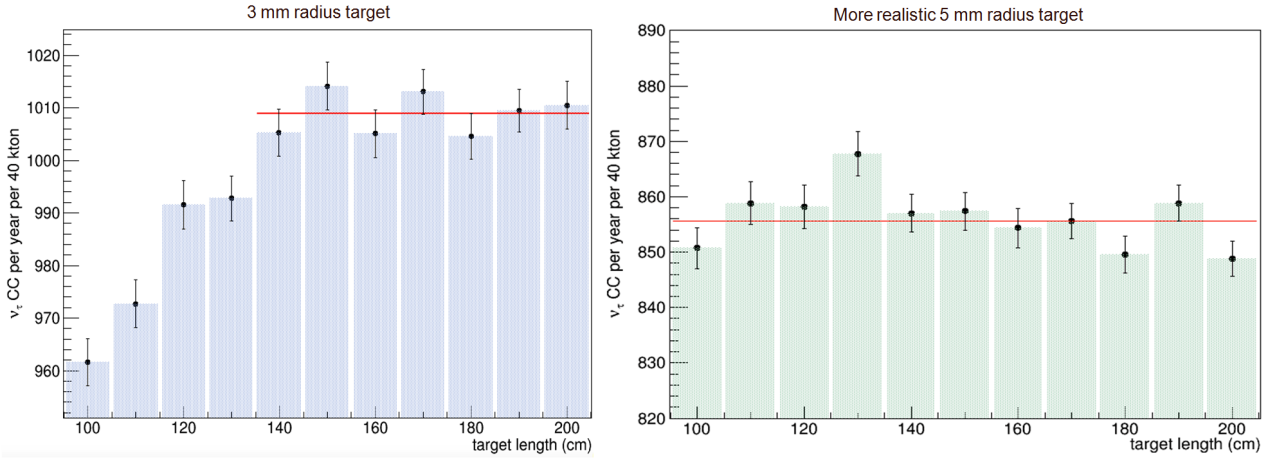

Good news for the 5-mm-radius cylindrical target; the events rate does not vary significantly with the target length.

Finally, I run a simulation using a 5-mm-radius 1.5-m-long cylindrical target with horn 2 radially rescaled by 70%, longitudinally rescaled by 80% and placed 18.3 m far from the zero. This configuration appeared to be the best after removing the command that was fixing the neck's diameter[3]. I got 887 ± 5 events, about $3 \pm 1\%$ more events compared to the result in the histogram above.

[3]See section 6.3

Chapter 7

Neutrino flux analysis

The histograms below represent the ν_μ flux for different positions of both the target and the second horn. Data belong to the simulations reported in section 6.2 (NuMI target, horn 2 not rescaled).

As the target is moved farther, the ν_μ flux decreases in height and becomes more energetic. Horn 1 captures less neutrinos but the neutrinos focused and straightened are more energetic.

In fact, as proven in section 2.2.2, the ratio p/f is constant for a parabolic horn, where p is the modulus of the charged particle momentum and f_1 is the focal length of the first horn, that is the distance between the neutrino-parent-particle vertex (assuming it was born into the target) and the horn's neck, in the thin-lens-approximation.

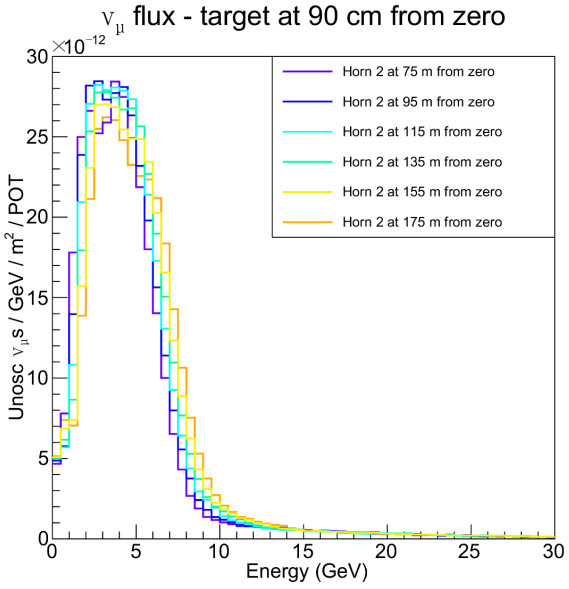

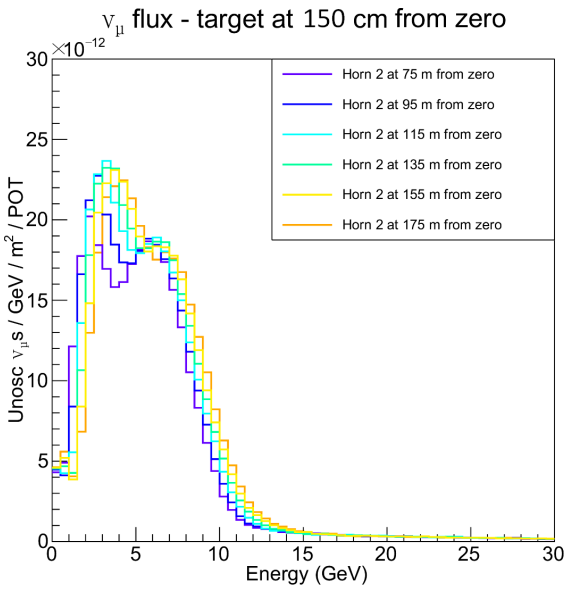

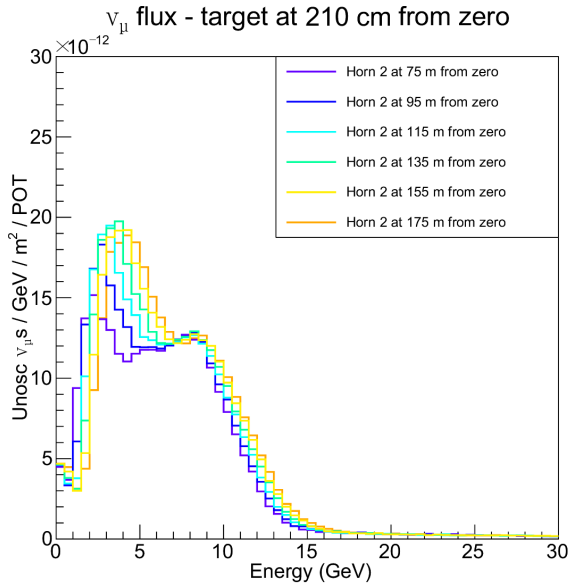

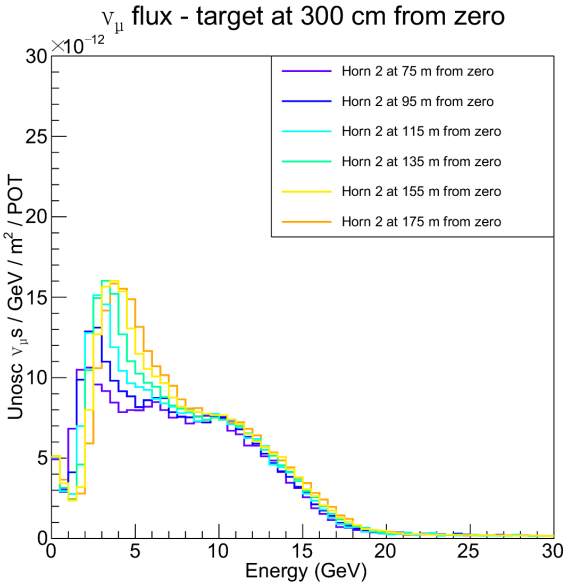

Increasing the target's z-offset means increasing the average parent-vertex-z-coordinate therefore the focal length f_1 and hence the average momentum of the well focused charged particles. Be f_2 the focal length of the second horn. Again, increasing f_2 means increasing the mean energy of the charged particles that can be focused by the second horn. With the target at 300 cm from zero, moving horn 2 further from horn 1, the flux not only shifts to the right, but it also increases for lower energies. Probably the energy spectrum of the charged particles coming from horn 1 is so high that horn 2 defocuses less energetic pions if placed too close to horn 1.

One can see that after moving the target and the second horn the flux develops a double peak. To understand the nature of the double peak I tried to separate different contributions to the flux.

The histogram below has been made to understand the distribution of neutrinos coming from different types of parent particles. Here the ν_μ flux refers to the sum of all the 100 simulations made for the 5-mm-diameter 1 m long cylindrical target (see section 6.4.2). Almost all the neutrinos come from positive charged pions (in the neutrino mode).

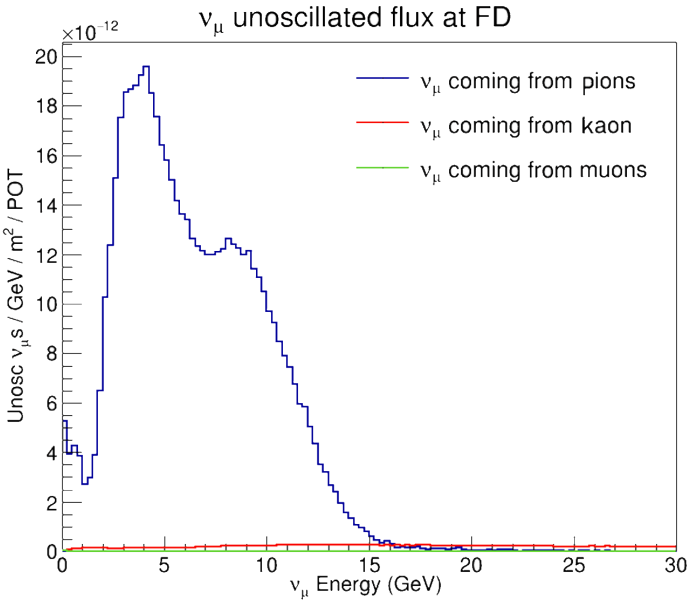

All the information available to understand how the neutrino flux is composed are contained into the ntuple and its branches. It came out that the separation of the single peak[1] into 2 peaks as the target is moved away is only due to geometrical factors and in particular on how the neutrino-parent-particles enter horn 1.

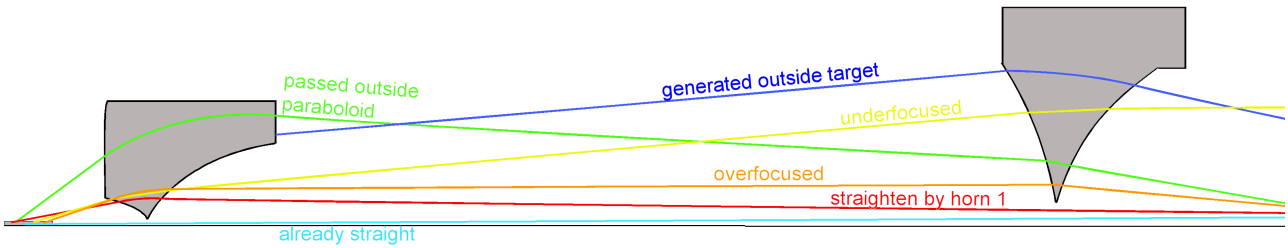

Figure 7.1: different pions trajectories

In the subsequent ν_μ flux histogram and ν_τ CC events rate I only selected neutrinos coming from pions, for simplicity.

Consider the most likely chance in which a pion is produced into the target. I split the pions produced inside the target by those generated outside the target, represented by a blue line.

Then for every pion produced into the target I split the ones that enter straight into the paraboloid by those that pass from the external side of the horn that separates inner conductor and outer conductor. The latter are represented by a green line. I called *paraboloid* the virtual surface that lies on the inner conductor's surface but also includes the horns's neck.

[1] see the ν_μ flux for the default reference design in section 2.2.1

My next step was dividing into different curves the pions going straight into the neck of horn 1 from those entering in the inner conductor. The former are represented by a light-blue line. For this configuration, almost all the pions that enter in the first horn's neck also enter into the second horn's neck.

The red line represents pions that enter into the inner conductor of horn 1 and then into the second horn's neck. Pions of about 8 GeV are well focused by the first horn. They have been produced mainly in the first half of the target, on average 250 cm far from the neck of horn 1. Thus the constant p/f is about 31 GeV/cm for the first horn.

At this point I still had a double peak involving the pions that went through both horn 1 and horn 2 paraboloid. I separated under-focused pions from over-focused pions, where *under-focused* means that the direction of the pion's momentum in his production vertex is the same as the direction of the pion's momentum in the neutrino vertex, while *over-focused* means that the opposite[2].

Moreover, nothing prohibits a low energy pion to be over-focused by both horns, so that it appears as it is under-focused; those pions could form the little yellow bump at 3.5 GeV in the ν_μ flux histogram.

The yellow curve is more energetic than the orange one and also more energetic than the red one. It refers to neutrinos generated by under-focused pions, too energetic to be focused by this system of horns. As for a two converging lens system, it is like yellow pions are produced before the focus of the lens system, while orange pions are produced after the focus and red pions are produced near the focus, except that the focus of a horn system depends of the particle momentum.

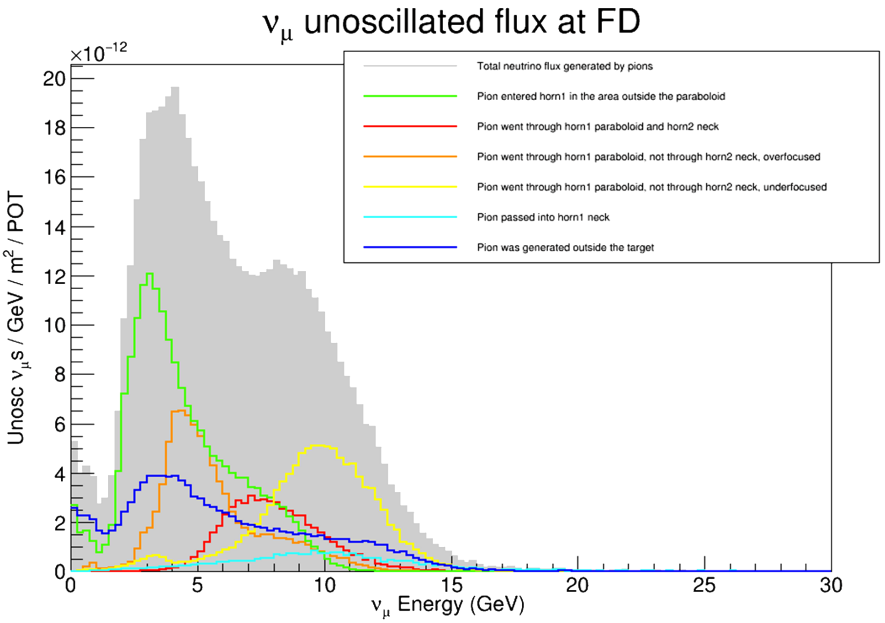

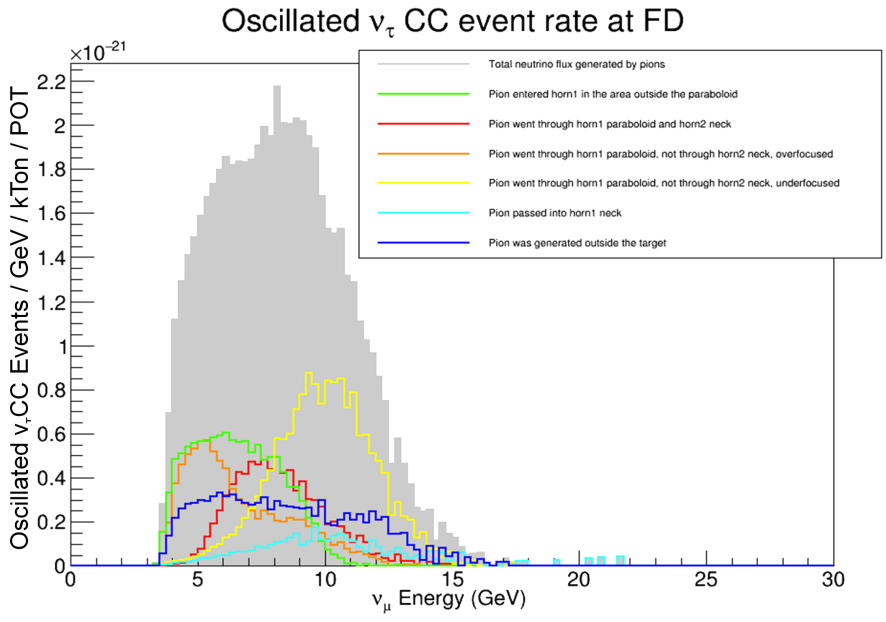

[2]Be $\vec{p}$ the momentum of the pion in his production vertex and $\vec{q}$ the momentum of the pion when it decays, in the neutrino vertex. if $p_x q_x + p_y q_y < 0$ then the pion is over-focused, else the pion is under-focused

Chapter 8

Conclusions

- The second horn has to be placed at the maximum distance allowed by the target hall size, id est 17.5 m far from the zero point.
- The target has to be placed about 2 m distant from the first horn.
- An previous study by Michael Dolce, intern at Brookhaven National Laboratory, carried out with a prior and different version of G4LBNF (G4LBNE v2) and with another cross-section simulator (GLoBES, General Long Baseline Experiment Simulator) also concluded that the optimal tune for ν_τ appearance for the reference NuMI-like focusing system is with the horn 2 at the maximum distance allowed by the target hall and with the target placed at 2 m from horn 1. This strengthen the goodness of the simulation code.
- The second horn has more focusing power if radially rescaled of about 75% and maybe also longitudinally rescaled. This would allow to put horn 2 even more distant (to 18.7 m from zero if longitudinally rescaled by 80%).
- A thinner target with low density works better and also it can be made longer without reducing significantly the number of events. In some cases a longer target increases the number of events. This is good because a longer target means less energy deposited in the absorber.
- A target that produces more pions from primary p^+ interactions is needed; this can be achieved by lowering the target density. An alternative target could be a cylindrical target composed by little cylinders separated by thin gaps of air. A target like this would reduce the probability of re-interactions, producing more high energy pions and so more high energy neutrinos.
- For the same reason (less probability of re-interactions) the multi spheres array target (SAT) was though to be more performing than the cylindrical one. Actually, if we compare the 13-mm-diameter SAT to the 6.5-mm-radius cylindrical target, the spherical target is more performing. It would be interesting to see what happens with 10-mm-diameter spheres, assuming that there aren't engineering problems in their construction. To compare the cylindrical and the SAT target it would be also necessary to chose graphite as the material for the spheres.
- A genetic algorithm or some other algorithm that takes into account multiple parameters should be implemented in order to find the very best configuration starting from a set of parameters found previously.
- The ν_μ flux can provide information on how to eventually modify the horns to ensure a better focusing. For instance, the green line, despite it has its peak at low energies, gives a significant contribution to the ν_τ events rate, but this contribution could probably be higher. Maybe some high energy pions composing the green line are not well focused due to the fact that they enter the magnetic field passing through an area where the optical laws of a parabolic horn do not wholly apply. Perhaps making the paraboloid facing the beam a little longer it would be possible to fine focus more high energy pions.
- A lot of work on the reconstruction efficiency has to be done. Anyway, even in the worst assumption in which the LarTPC reconstruction efficiency is 10%, and only from the results of this preliminary optimization, about $850 * 0.867 * 0.1 = 74$ events per year can be reconstructed.

Bibliography

[1] Dune Collaboration,"DUNE/LBNF CDR Volume 2: The Physics Program for DUNE at LBNF" (2016)

[2] Dune Collaboration, "DUNE/LBNF CDR Volume 1: The LBNF and DUNE Projects" (2016)

[3] B. Pontecorvo, S.M. Bilenky, "Lepton mixing and neutrino oscillations" (1977)

[4] Sacha E. Kopp,"Accelerator neutrino beam" (2006)

[5] A. Marchionni,"Status and New Ideas Regarding Liquid Argon Detectors" (2013)

[6] Opera Collaboration, "Evidence for $\nu_\mu \to \nu_\tau$ appearance in the CNGS neutrino beam with the OPERA experiments" (2014)

[7] Nomad Collaboration, "A search for $\nu_\mu \to \nu_\tau$ oscillations using the NOMAD detector" (1998)

[8] A. Marchionni, "Results from DONUT" (1998)

[9] Particle Data Group, "14. Neutrino mass, mixing and oscillations" (2016)